Two-Stage Mafic-Felsic Magma Interactions and Related Magma Chamber Processes in the Arc Setting: An Example from the Enclave-Bearing Calc-alkaline Plutons, Chinese Altai

Xing Cui[1], Min Sun[1], Guochun Zhao[2], Yunying Zhang[3], and Jinlong Yao[4]

[1]University of Hong Kong
[2]Department of Earth Sciences, the University of Hong Kong
[3]University of HongKong
[4]Northwest University

November 23, 2022

Abstract

A systematic dataset of petrography, mineralogy, geochronology, and geochemistry is reported for the enclave-bearing calc-alkaline I-type granitoids from the Chinese Altai, Central Asian Orogenic Belt (CAOB). Zircon U–Pb dating and geochemical data indicate that the MME and granitoids formed coevally at ˜395 Ma in a subduction setting. Geochemical modelling and hybrid testing suggest that the granitoid parental magma was formed by mixing between a mafic and a felsic endmember that can be identified by isotopic compositions. The mafic rocks have $(^{87}Sr/^{86}Sr)_i$ of 0.7048 – 0.7062, εNd(t) of -0.5 – +2.6, and zircon εHf(t) of +2.3 – +5.4, while the host granitoids have similar Sr isotopic compositions ($(^{87}Sr/^{86}Sr)_i$ = 0.7054 – 0.7064), but generally lower whole-rock εNd(t) and zircon εHf(t) values (-2.2 – +0.4 and +0.6 – +4.6, respectively). The sharp decrease of An values from cores to rims (e.g., from ca. 80 to 40) of plagioclase phenocrysts points to polybaric crystallization accompanied by degassing, which is supported by the pressure and water content estimations based on amphibole compositions. Petrographic evidence and plagioclase in-situ Sr isotopic compositions ($(^{87}Sr/^{86}Sr)_i$ = 0.7053 - 0.7071) confirm the interaction of two isotopically different magmas during the mineral crystallization. A model for the formation of the enclave-bearing calc-alkaline plutons in an arc setting is presented: in-depth mantle and crustal melting and efficient magma mixing controlled the principal chemical compositions of the granitoid intrusions, while the later decompression-dominated crystallization, magma mingling and limited mixing in the higher crustal level finally determined the texture, mineral composition, and enclave morphology.

Hosted file

`essoar.10507295.1.docx` available at https://authorea.com/users/544908/articles/601873-two-stage-mafic-felsic-magma-interactions-and-related-magma-chamber-processes-in-the-arc-setting-an-example-from-the-enclave-bearing-calc-alkaline-plutons-chinese-altai

Hosted file

`agusupporting-information_word_template.docx` available at https://authorea.com/users/544908/articles/601873-two-stage-mafic-felsic-magma-interactions-and-related-magma-chamber-processes-in-the-arc-setting-an-example-from-the-enclave-bearing-calc-alkaline-plutons-chinese-altai

Xing Cui[1], Min Sun[1]*, Guochun Zhao[1,2], Yunying Zhang[1], and Jinlong Yao[2]

[1]Department of Earth Sciences, The University of Hong Kong, Pokfulam Road, Hong Kong, China.

[2]Department of Geology, Northwest University, Xi'an, 710069, China.

Corresponding author: Min Sun (minsun@hku.hk)

Key Points:

- Efficient magma mixing in the deep source zone controlled the principal chemical compositions of the granitoid intrusions.
- MME in granitoids are quenched mafic magma, having experienced mingling and limited mixing in the higher crustal level.
- Two stage mafic-felsic magma interactions were operated in the generation of enclave-bearing calc-alkaline granitoids.

Abstract

A systematic dataset of petrography, mineralogy, geochronology, and geochemistry is reported for the enclave-bearing calc-alkaline I-type granitoids from the Chinese Altai, Central Asian Orogenic Belt (CAOB). Zircon U–Pb dating and geochemical data indicate that the MME and granitoids formed coevally at ~395 Ma in a subduction setting. Geochemical modelling and hybrid testing suggest that the granitoid parental magma was formed by mixing between a mafic and a felsic endmember that can be identified by isotopic compositions. The mafic rocks have $(^{87}Sr/^{86}Sr)_i$ of 0.7048 – 0.7062, Nd(t) of -0.5 – +2.6, and zircon Hf(t) of +2.3 – +5.4, while the host granitoids have similar Sr isotopic compositions ($(^{87}Sr/^{86}Sr)_i$ = 0.7054 – 0.7064), but generally lower whole-rock Nd(t) and zircon Hf(t) values (-2.2 – +0.4 and +0.6 – +4.6, respectively). The sharp decrease of An values from cores to rims (e.g., from ca. 80 to 40) of plagioclase phenocrysts points to polybaric crystallization accompanied by degassing, which is supported by the pressure and water content estimations based on amphibole compositions. Petrographic evidence and plagioclase in-situ Sr isotopic compositions ($(^{87}Sr/^{86}Sr)_i$ = 0.7053 - 0.7071) confirm the interaction of two isotopically different magmas during the mineral crystallization. A model for the formation of the enclave-bearing calc-alkaline plutons in an arc setting is presented: the in-depth mantle and crustal melting and efficient magma mixing controlled the principal chemical compositions of the granitoid intrusions, while the later decompression-dominated crystallization, magma mingling and limited mixing in the higher crustal level finally determined the texture, mineral composition, and enclave morphology.

1 Introduction

Granitoids are principal constitutes of the felsic continental crust and their formation is of fundamental significance in interpreting the generation and evolution of the continental crust. The petrogenesis of granitoids has been hotly

debated for a long time, which invoked the complex interplay between several geological processes including fractional crystallization, crustal melting and/or assimilation, and magma mixing. A large number of calc-alkaline I-type granitoids occur in arc settings, which may signify the growth of the continental crust. Although plutonic bodies are usually homogeneous with imprints of operated magmatic processes largely obliterated, many of them preserve field and textural evidence consistent with hybridization of compositionally diverse magmas (e.g., *R. A. Wiebe,* 1993). For example, despite that MME (mafic microgranular enclaves) within granites may have different origins such as restite, autoliths/cognate fragments, and quenched globules of a mafic magma, those within the calc-alkaline plutons are mostly of igneous origin and sometimes associated with mafic dykes, and thus have been deemed as an archive for multiple magma involvement (*JD Blundy & Sparks,* 1992; *Browne et al.,* 2006; *Cheng et al.,* 2012; *DORAIS et al.,* 1990; *Kumar & Rino,* 2006; *Perugini et al.,* 2003; *Vernon,* 1983, 1984; *K. Yu et al.,* 2018). Therefore, the importance of mafic magmatism for the generation of calc-alkalic plutons and batholiths in convergent-margin settings is widely recognized. For example, some large batholiths from the Cordilleran arcs, such as the Sierra Nevada batholith in California (*Barbarin,* 2005; *Coleman et al.,* 2004; *Ratajeski et al.,* 2001) and the Coast Ranges in British Columbia (*Brown & McClelland,* 2000; *Gehrels et al.,* 2009) were proposed to grow incrementally with frequent recharge by mafic magmas in a million-year time scale.

Consequently, vigorous discussions have been centered on the role of magma hybridization in the petrogenesis of the calc-alkaline granitoids (e.g., *Barbarin,* 2005; *B. Chappell,* 1996; *Janoušek et al.,* 2004; *Slaby & Martin,* 2008; *R. Wiebe et al.,* 2002; *R. Wiebe et al.,* 1997). Nevertheless, the condition and mechanism concerning location, timing, and detailed process of the hybridization between two compositionally different magmas are complex and become a continuing topic of debate. With additional difficulties to ascertain the magma source and generation, and the magma chamber geometry and processes, contrasting models have been proposed for the formation and evolution of granitoid suites in arc settings (e.g., *Annen et al.,* 2006; *Castro et al.,* 2010; *Bruce W Chappell & White,* 2001; *Grove et al.,* 2003; *Janoušek et al.,* 2004; *Poli et al.,* 1996; *T. W. Sisson et al.,* 2005; *Turnbull et al.,* 2010; *Vernon,* 1984; *Zhang et al.,* 2016). To better understand how magmatic systems evolve and to furnish a general evolutionary model of the enclave-bearing batholith/pluton in arc settings, we emphasize the need for an integrated study on arc granitic bodies with preserved disequilibrium textures, using a multi-faceted approach that involves field investigation, petrographic observation, as well as mineral and whole-rock geochemistry.

The Chinese Altai underwent extensive arc-related magmatic activities in the Paleozoic. The Tuerhongnan Batholith (TB) and Chaergan Pluton (CP), products of such activities, are typical calc-alkaline I-type granitoids with Na_2O-rich, metaluminous to weakly peraluminous chemical characteristics. Their close relationship with mafic magmatism, as manifested by the widely distributed MME and mafic dyke intrusions, makes them excellent examples of coeval mafic and

felsic magmatism in a continental arc setting. In this study, a combination of petrography, whole-rock chemical analysis, and in-situ elemental and isotopic composition determination for minerals (1) provides a deeper insight into the nature of magma sources and magma generation processes; (2) unravels the felsic-mafic magma interactions operated within 'magma chambers' at both source region and high emplacement level; and (3) better refines the integrated evolutionary model of the studied calc-alkaline igneous suites from generation to emplacement.

2 General Geology of the TB and CP and Samples

The TB and CP are located in the eastern range of the Chinese Altai, a tectonic unit of the CAOB that represents one of the largest accretionary-type orogenic belts in the Phanerozoic (Fig. 1a; e.g., *Şengör et al.,* 1993; *Windley et al.,* 2007; *Xiao et al.,* 2009). Comprehensive research on the Chinese Altai orogen involving magmatism, metamorphism, and structural deformation has revealed its formation by northward subduction-accretion of the Paleo-Asian Ocean in the early Paleozoic, which continued until the collision with the southernly Junggar arc in the Carboniferous-Permian (e.g., *Broussolle et al.,* 2018; *Li et al.,* 2017; *Sun et al.,* 2009; *Sun et al.,* 2008; *Y. Wang et al.,* 2014). Prolonged orogenic history since the Cambrian produced extensive magmatic activities, including voluminous granitoids and subordinate mafic intrusions, which characterize the Chinese Altai orogenic belt. Early Paleozoic I-type granitoids, mainly distributed in the central and northern part of the Chinese Altai, have been interpreted as products of the ongoing subduction in an active continental margin (*Sun et al.,* 2008; *T. Wang et al.,* 2006; *Yu et al.,* 2017b; *Yuan et al.,* 2007). Many of them are loaded with MME, especially those close to coeval mafic complexes, among which are the TB and CP in this study.

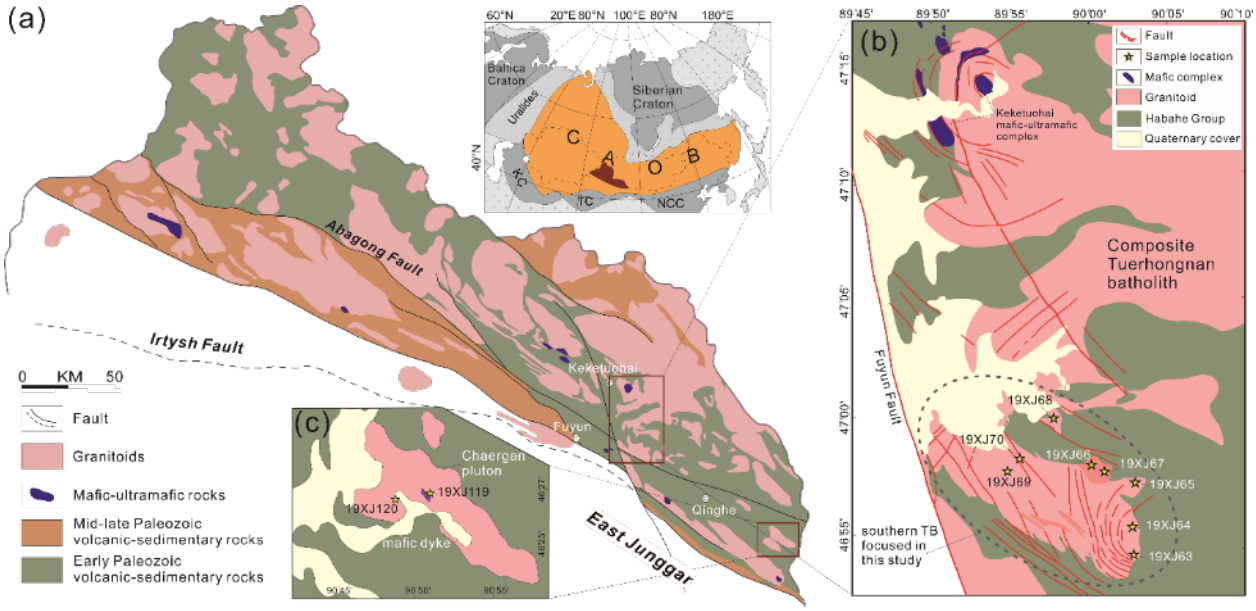

Figure 1. (a) Geological map of the Chinese Altai orogen (modified after *Windley et al.,* 2002; *Broussolle et al.,* 2019). Insert small figure at top center is the sketch map of the CAOB, with red area indicating the location of the Chinese Altai. KC – Kalakumu Craton; TC – Tarim Craton; NCC – North China Craton. (b) Simplified geological map of the Tuerhongnan Batholith (TB) and relationship with adjacent igneous suites (modified after Keketuohai Geological Map at 1:100,000 scale, 2013). (c) Simplified geological map of the Chaergan Pluton (CP). Sample locations are shown in (b) and (c).

The TB is one of the typical syn-subduction intrusive complexes of the Chinese Altai (Fig. 1a). It is a composite batholith composed of multiple magma batches lasted from ca. 410 to 360 Ma, occupying a huge area of about 1,200 km^2 (*Yuan et al.,* 2007), and in this study we focus on its southern part (Fig. 1b). It intruded into the early Paleozoic Habahe Group, which represents the oldest terrigenous and volcano-sedimentary rocks in the Chinese Altai orogen (*Jiang et al.,* 2016; *Long et al.,* 2008). MME are unevenly distributed in the TB, with a mafic complex (called Keketuohai mafic complex, *Cai et al.,* 2012) exposed in the northern region (Fig. 1b). The MME in the TB cluster as swarms in some places while scatter or disappear in other locations. They are typically ellipsoidal, rounded or irregular in shape with varying sizes ranging from ca. 4 to 50 cm, showing either sharp or diffusive contacts with the host granitoids (Fig. 2). To the southeast of the TB, the CP outcrops as a NW-SE elongated body and intrudes into the Habahe Group as well (Fig. 1c). MME in the CP do not significantly differ in the morphology or size from those in the TB, and associated gabbroic dyke intrudes the CP.

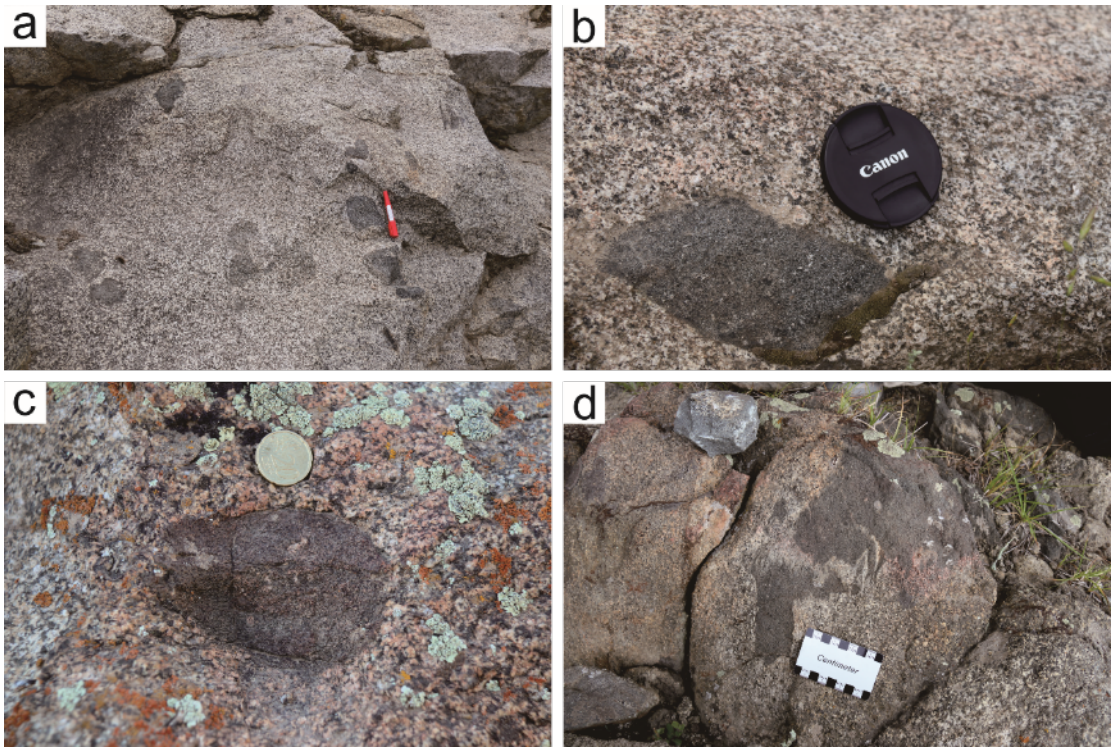

Figure 2. Field photographs of the enclave-granitoid associations from the TB and CP. (a) shows the enclave swarm; (b), (c), and (d) show the various shapes of the MME and their contact relationships with host rocks.

The light-colored host rocks and dark-colored enclaves/dyke are respectively referred to as felsic granitoids and MME/mafic dyke in this study, although in each group they gradually transit to intermediate chemical compositions. Granitoids from the TB can be classified into dominant biotite-granodiorite and subordinate quartz diorite according to the relative proportions of biotite and amphibole. The amphibole-free samples (19XJ63-1, 65-1, 68-1, 69-1, 70-1) are porphyritic with large phenocrysts of plagioclase and biotite (ca. 1-2.5 mm) enclosed in a matrix of plagioclase, quartz, and K-feldspar. Averaged mineral proportions are ca. 35 % plagioclase, 20 % K-feldspar, 25-30 % quartz, 10-15 % biotite, and minor accessories including apatite, titanite, zircon, Fe-Ti oxides, and epidote (Fig. 3a). Plagioclase phenocrysts are euhedral to subhedral, zoned prismatic crystals, and sometimes show synneusis grouping. Many of them have distinct core-rim textures, with the core more severely altered into secondary minerals (Fig. 3g and h; Fig. 16a and b). Biotites appear in two different forms (Fig. 3a). One type is large subhedral bladed crystals with small mineral inclusions, showing a primary magmatic origin. The other type appears as aggregates of

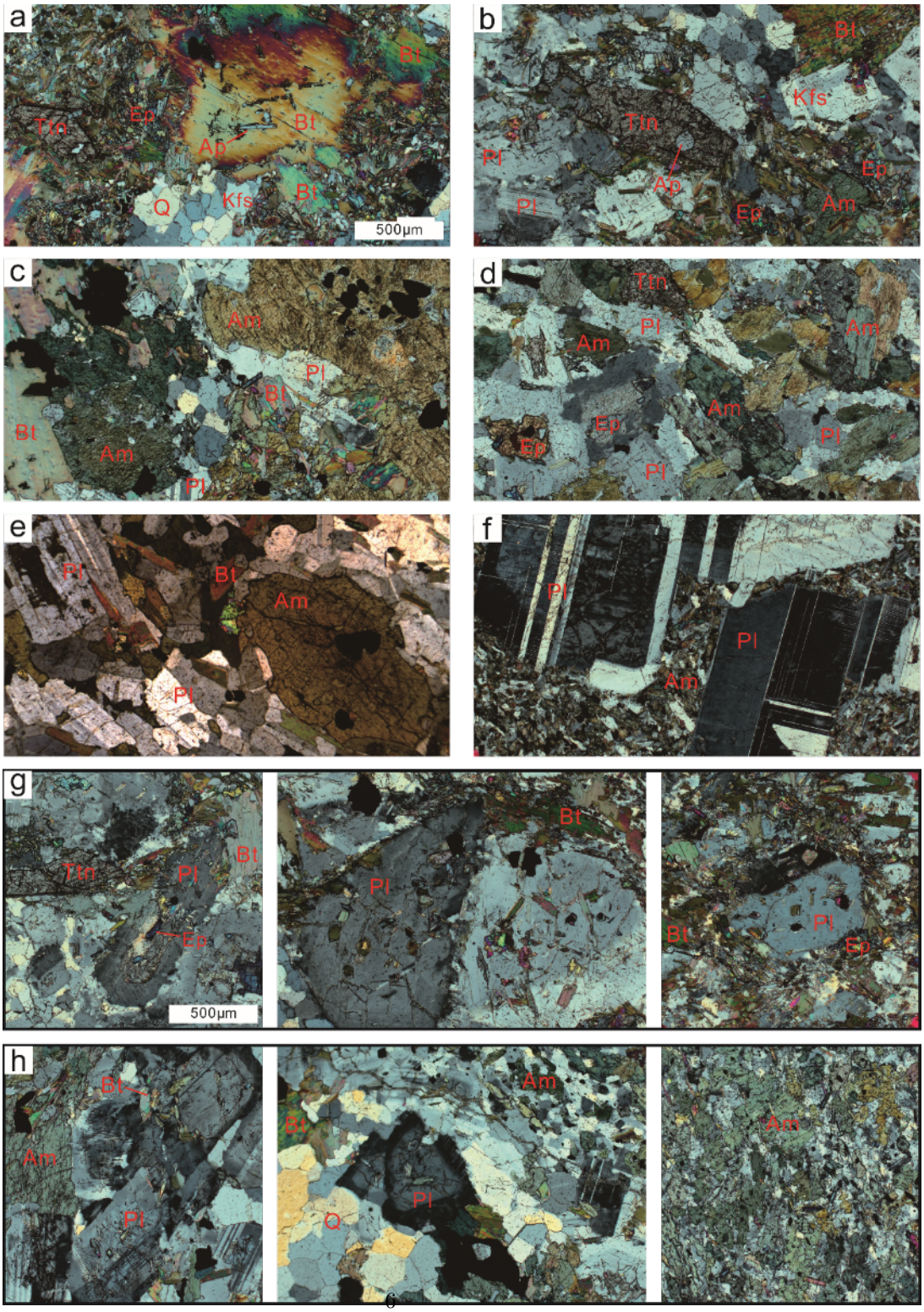
a
Bt
Ttn
Ep
Bt
Ap
Q
Kfs
Bt
500μm
b
Bt
Kfs
Ttn
Pl
Ap
Ep
Pl
Ep
Am
c
Am
Pl
Bt
Bt
Am
Pl
d
Ttn
Pl
Am
Am
Ep
Am
Ep
Pl
Pl
e
Pl
Bt
Am
Pl
f
Pl
Pl
Am
g
Ttn
Pl
Bt
Ep
500μm
Bt
Pl
Bt
Pl
Ep
h
Bt
Am
Am
Pl
Bt
Am
Q
Pl
Am

Figure 3. Cross-polarized light photomicrographs of the granitoids, MME, and mafic dyke from the TB and CP. (a) Biotite-granodiorite sample (19XJ63-1) from the TB. Primary biotite with resorption surface is juxtaposed with hydrothermal biotites, which appear as aggregates of fine-grained flakes intergrown with tiny epidote. (b) Amphibole-bearing biotite-granodiorite sample (19XJ64-6) from the TB. (c) Quartz diorite sample (19XJ66-1) from the TB. Large, tabular amphiboles show blue-green and yellow-brown pleochroism. (d) Gabbro-dioritic MME sample (19XJ64-1) from the TB. Amphiboles are isolated subhedral crystals. (e) Hornblende-gabbroic MME sample (19XJ119-4) from the CP. Lath-shaped plagioclase show some alignment and cumulative texture. (f) Hornblende-gabbroic dyke sample (19XJ119-7) intruding into the CP. Large plagioclase phenocrysts are xenocrysts and interspersed in the fine-grained matrix. (g) and (h) are thin sections where enclave and host rocks coexist, with host granitoids on the left, transition zone in the middle, and MME on the right. (g) (sample 19XJ64-4) is biotite-granodiorite and associated MME, and plagioclase phenocrysts in the transition zone and enclave side suggest crystal transfer between the two sides. (h) (sample 19XJ63-3) is quartz diorite and associated MME, showing planar interface with obvious crystal size difference between the two sides. Mineral abbreviations: Am – amphibole; Ap – apatite; Bt – biotite; Ep – epidote; Kfs – K-feldspar; Pl – plagioclase; Q – quartz; Ttn – titanite.

fine-grained flakes, intergrown with epidote and opaque minerals and usually adjacent to the tabular biotite phenocrysts. It suggests that they are most likely hydrothermal biotites (*Idrus,* 2018), replacing the early primary ones and sometimes forming pseudomorphs up to 5 mm. Unzoned plagioclase, cross-hatched K-feldspar, and quartz in the matrix are subhedral, granular, and 0.1-0.5 mm. Amphiboles appear in one biotite-granodiorite sample (19XJ64-6; Fig. 3b) as subhedral phenocrysts (about 5 %). Quartz diorite samples (19XJ66-1, 66-4, 67-1, 67-2) have more amphibole than biotite, with average mineral assemblages of plagioclase (40-45 %), amphibole (20 %), quartz (15 %), K-feldspar (5-8 %), biotite (10 %), and accessories (<5 %). Amphiboles show blue-green and yellow-brown pleochroism, appearing either as euhedral isolated crystals or large, tabular, and poikilitic crystals with plagioclase embedded in. Granitoids from the CP have similar mineral assemblages to biotite-granodiorite from the TB, with varied mineral proportions of plagioclase (35-50 %), K-feldspar (10-30 %), quartz (20-30 %), biotite (3-15 %), and minor accessories (<3 %).

The mafic enclaves from both TB (Fig. 3c and d) and CP (Fig. 3e) have identical mineral associations to their respective host rocks but possess higher contents of mafic minerals and finer-grained textures. They are mostly inequigranular, consisting of 0.2-1 mm plagioclase and amphiboles with micro inclusions, and <0.2 mm anhedral plagioclase, quartz, and scarce K-feldspar. Magmatic foliations and typical igneous textures such as interstitial and poikilitic minerals with oscillatory zoning suggest that they were crystallized from magmas (*Barbarin,* 2005; *Y. Yu et al.,* 2018) but not restite fragments (*B. W. Chappell et al.,* 1987). As shown in thin sections with enclave and host rock in contact (Fig. 3g and h), felsic materials often penetrate into the enclave, and the interface

between them is typically planar with contrasts of mineral proportion and grain size. The mafic dyke intruded the CP has the same modal mineralogy as the enclaves. It shows a porphyritic texture (Fig. 3f), characterized by a homogeneous matrix composed of finer-grained plagioclase and amphibole crystals (ca. 0.1-0.2 mm) interspersed with ca. 3-5 mm plagioclase phenocrysts, suggesting a possible crystal transfer with host rocks and thus a syn-plutonic character.

Common accessory titanite in both granitoids and MME shows euhedral-subhedral wedge or irregular shapes with lengths of ca. 0.5-0.8 mm, while apatite displays either tiny acicular habits as inclusions in most major mineral phases or isolated intergranular tabular shapes with lengths up to 0.7 mm. Epidote stands out with high interference color, typically <0.2 mm inside the plagioclase cores or intergrown with biotite clots. Other trace minerals include sericite, muscovite, and kaolinite, which are products of secondary alteration and often replace the core of feldspar. Petrographic observation demonstrates that the TB was more severely altered than the CP, while the MME were more severely altered than the host granitoids.

3 Analytical Methods

Whole-rock major-trace elements and Sr-Nd isotopes, zircon U-Pb and Lu-Hf isotope systematics, mineral in-situ elemental and plagioclase in-situ Sr isotopic compositions were determined for the selected igneous rocks of the TB and CP. Full details of analytical methods are provided in supporting information.

4 Results

4.1 Zircon U-Pb geochronology and in-situ Hf isotope

Zircons from the granodiorite sample (19XJ63-1) from the TB are short prismatic euhedral crystals with lengths of ca. 80-120 m. They are characterized by clear oscillatory zonings with thin dark rims and Th/U ratios of 0.14-1.12. Twenty-one of them have clustered $^{206}Pb/^{238}U$ ages of 382-402 Ma, giving a weighted mean of ca. 394.6 ± 2.6 Ma (Fig. 4a). The clustered magmatic zircons of ca. 395 Ma give Hf(t) values of +1.6 to +4.5 and a narrow range of T_{2DM} between 1.08 and 1.26 Ga (Fig. 5).Three additional analyses yield $^{206}Pb/^{238}U$ ages of 611, 617, and 1044 Ma, which are thought to be xenocrysts from country rocks, and their variable Hf(t) values range from -4.3 to +5.4.

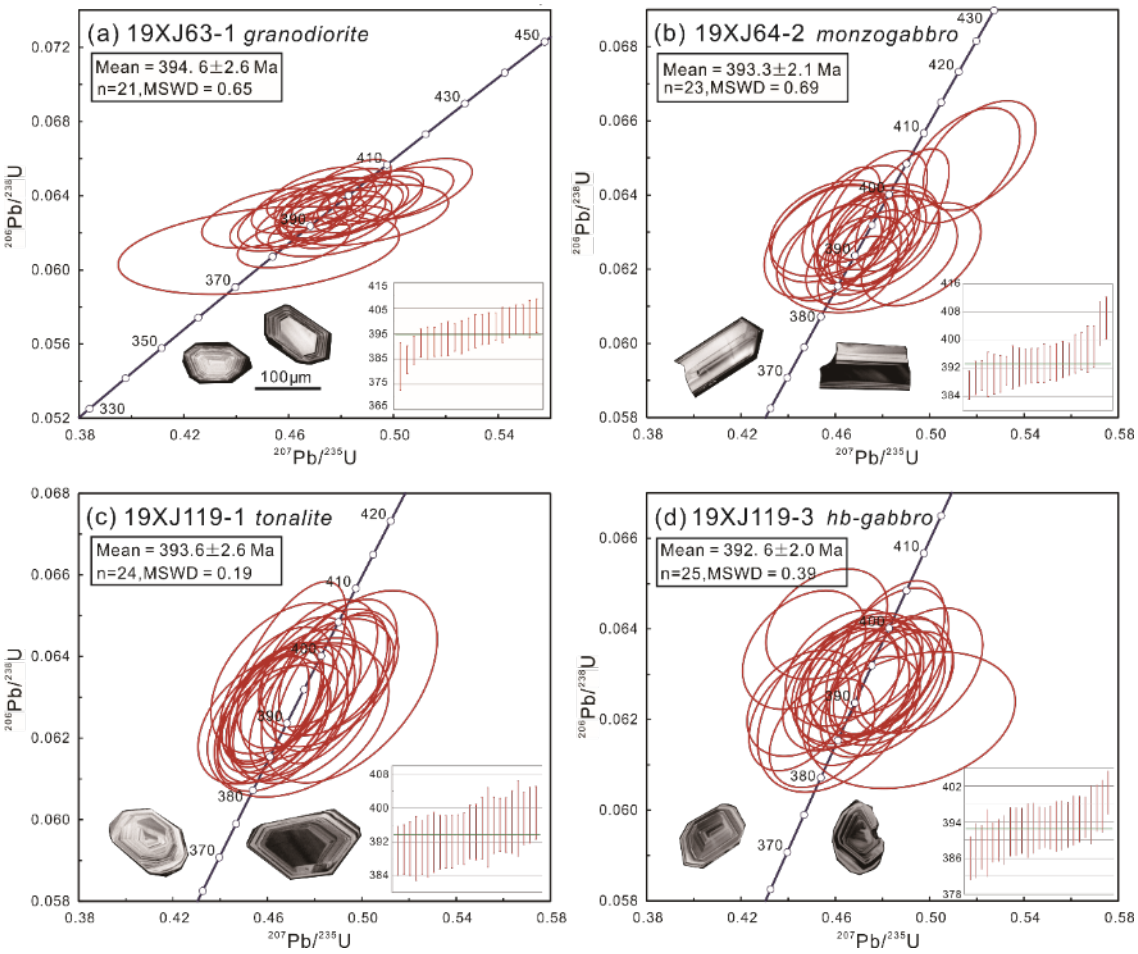

Figure 4. Concordant plots of LA-ICP-MS zircon U–Pb dating results for host granitoids and MME from the TB (a and b) and CP (c and d).

Zircons from the enclave (19XJ64-2) of the TB have mostly euhedral, elongated lath shapes (100-200 m) with visible zonings and high Th/U ratios of 0.34-1.59. Twenty-three analyses give well-grouped concordant $^{206}Pb/^{238}U$ ages, which range from 387 to 406 Ma and yield a weighted mean of ca. 393.3 ± 2.1 Ma (Fig. 4b). In-situ Hf isotopic analyses yielded Hf(t) values of 2.8-5.4 and T_{2DM} of 1.02-1.19 Ga (Fig. 5).

Zircons from the tonalite (19XJ119-1) of the CP are euhedral, granular or elongated with variable lengths of 80-250 m. They have clear oscillatory zonings with Th/U ratios of 0.59-1.06. Twenty-four dated grains give consistent $^{206}Pb/^{238}U$ ages of 390-399 Ma, with a weighted mean of 393.6 ± 2.6 Ma (Fig. 4c). Zircons from this sample have Hf(t) values of 0.6-4.6 and T_{2DM} of 1.07-1.32 Ga (Fig. 5).

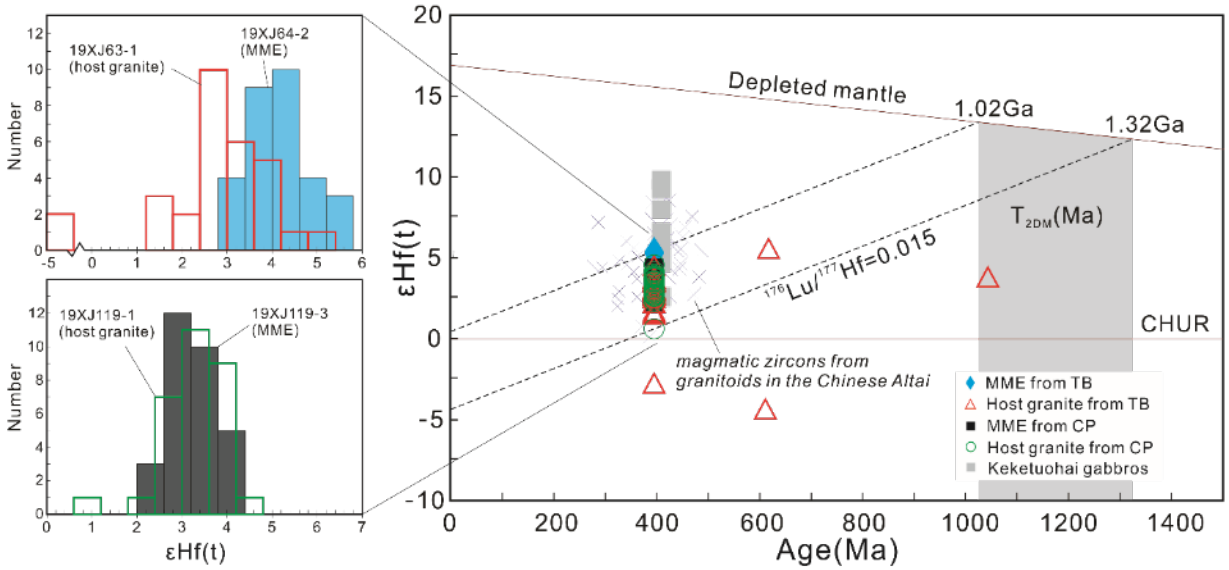

Figure 5. Zircon Hf isotopic data for the dated granitoid and MME samples from the TB and CP. On the left are histograms of the Hf(t) values of zircons (TB in the top and CP in the bottom). On the right is the Hf(t) values vs. Age (Ma). CHUR = chondritic uniform reservoir. The sample symbols are consistent with figure 6. Data for Keketuohai mafic complex are from *Yu et al.,* 2017a, and for granitoids in the Chinese Altai are from *Cai et al.,* 2011.

Zircons from the MME (19XJ119-3) of the CP have prismatic shapes, 80 to 200 m long, with slightly rounded margins or erosional boundaries. Oscillatory zonings and Th/U ratios of 0.59-1.25 indicate their magmatic origins. Twenty-five zircon grains have limited $^{206}Pb/^{238}U$ ages between 386 and 401 Ma, with a weighted mean of 392.6 ± 2.0 Ma (Fig. 4d). The thirty zircon-Hf analyses show restricted variations of Hf(t) values (2.3-4.2), and T_{2DM} (1.10-1.22 Ga; Fig. 5).

High-resolution zircon U-Pb dating of the above four representative samples reveals that: (1) the MME and their host granitoids from both the TB and CP have the same crystallization ages within analytical error, and (2) the emplacement of the TB and CP were coeval, possibly responding to one common tectonic event in the Chinese Altai.

4.2 Mineral compositions

Both the amphibole and biotite from the felsic and mafic rocks show overlapped compositions. The analyzed amphiboles are all calcic in composition (Ca_B>1.5), ranging from

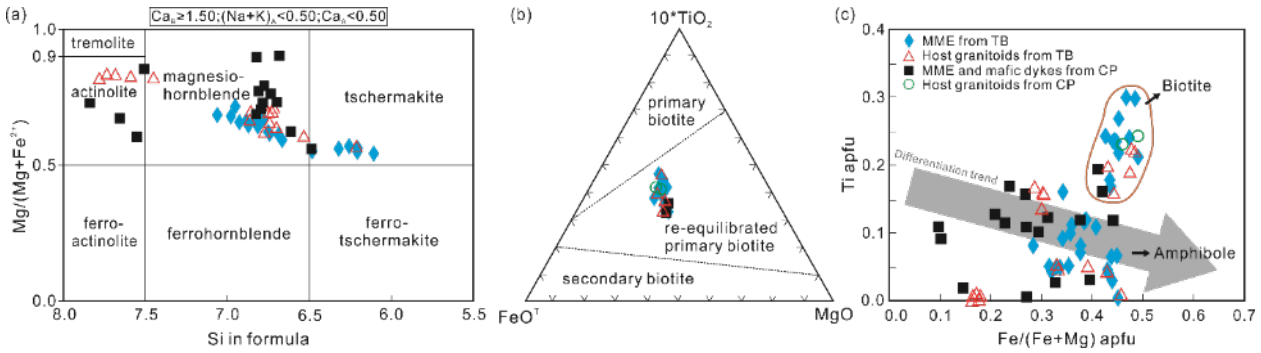

Figure 6. Chemical compositions of amphibole and biotite from mafic-felsic rocks of the TB and CP. (a) Plot of calcic amphibole compositions from *Leake et al.,* 1997. (b) FeO – 10*TiO_2 – MgO ternary diagram from *Nachit et al.,* 2005. (c) Variation of Ti vs. Fe number for biotite and amphibole after *Slaby & Martin,* 2008.

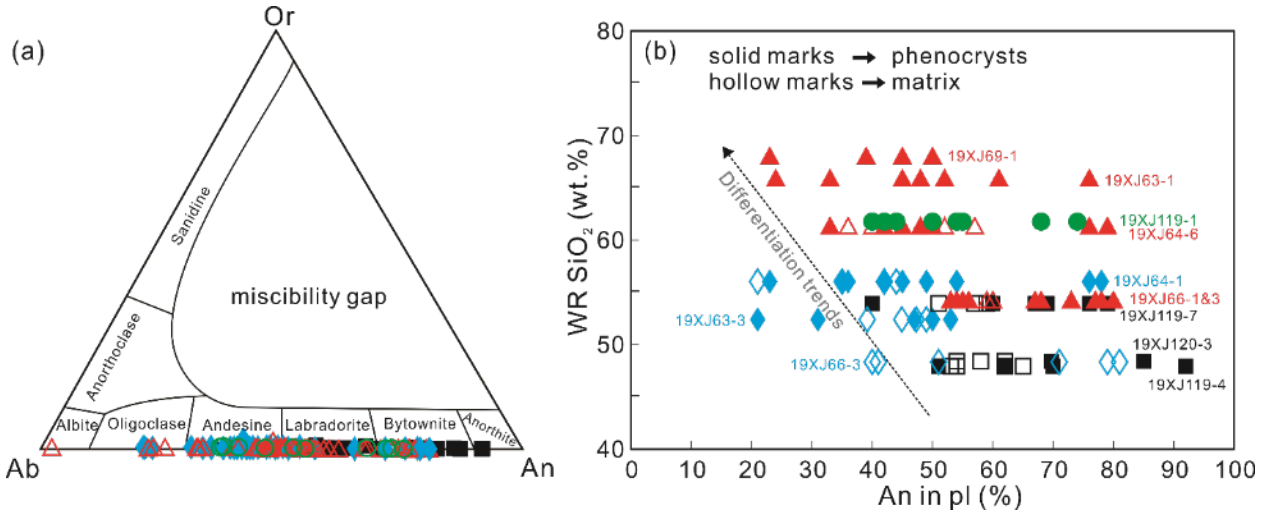

Figure 7. Chemical compositions of plagioclase from mafic-felsic rocks of the TB and CP. The sample symbols are consistent with figure 6. In the 7b, analytical spots in the sample 19XJ66-3 with co-existent enclave and host rocks are represented by red triangle symbols for the granitoid side and blue diamond symbols for the MME side. Their WR (whole-rock) SiO_2 contents adopt the value for 19XJ66-1 (granitoid) and 19XJ66-2 (MME), respectively.

tschermakite through magnesio-hornblende to actinolite (Fig. 6a). They have low and variable TiO_2 contents of 0-1.5 wt% and Fe number of 0.1-0.5, showing a differentiation trend and some alteration (Fig. 6c). The analyzed biotites are all tabular phenocrysts, not tiny crystal aggregates. They have FeO contents of 15.9-18.7 wt%, MgO of 10.3-13.3 wt%, and TiO_2 of 1.4-2.6 wt%, plotting into the re-equilibrated primary biotite field in the discrimination diagram, suggesting a

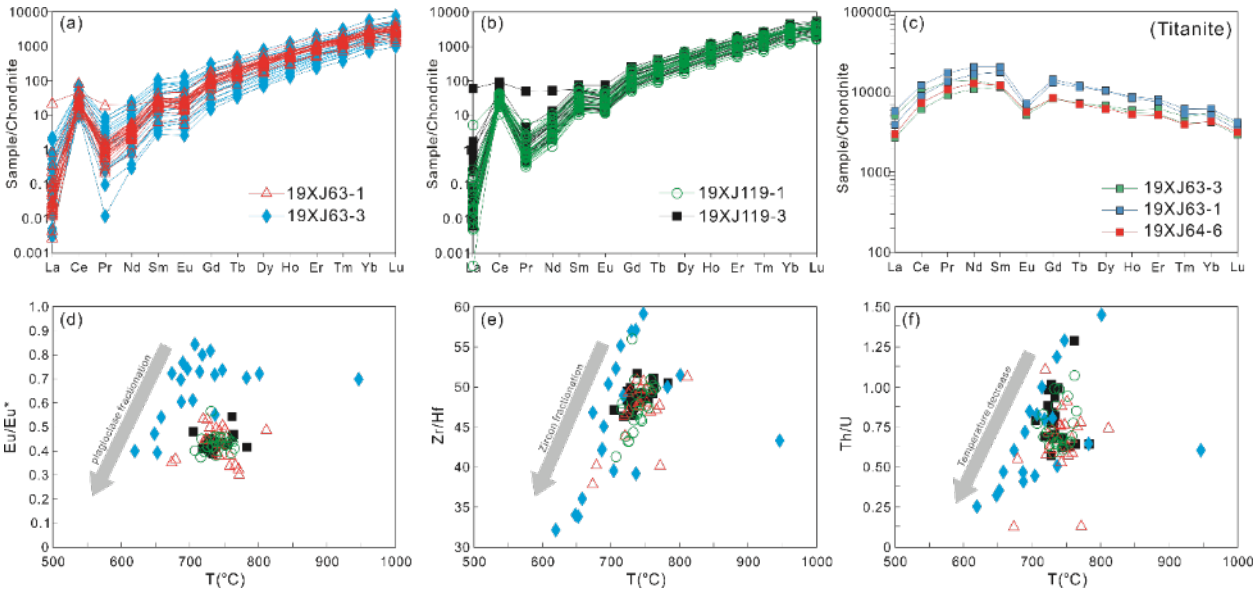

Figure 8. Chemical compositions of accessory minerals from mafic-felsic rocks of the TB and CP. (a)-(c) are REE diagrams respectively for zircons from TB samples, zircons from CP samples, and titanite from TB host granitoids (19XJ63-1 and 64-6) and MME (19XJ63-3). (d)-(f) are plots of zircon trace elemental ratios vs. Hf-in-zircon temperatures, modified after Yan *et al.* (2018).

cation exchange in the later stage (Fig. 6b and c). Plagioclase from the host granitoids ranges from oligoclase to bytownite with An values between 22.1 and 80.7, while those from the enclaves have a larger variation from oligoclase to anorthite with An of 23.1-91.6 (Fig. 7a). They show a continuous compositional trend from the most mafic enclave to the most felsic host granite despite large variations within individual samples (Fig. 7b).

Chondrite-normalized REE patterns of the zircons are generally parallel with a steep positive slope defined by HREE enrichment over LREE, accompanied by positive Ce and weak or without negative Eu anomalies (Fig. 8a and b). Excluding the captured xenocrysts and some with abnormally high values that may be associated with unexpected inclusions, Ti concentrations in the zircons from granite sample 19XJ63-1 (4.67-19.3 ppm) yield temperatures from 679 to 812 °C based on the Ti-in-zircon thermometer in *Ferry and Watson* (2007). Zircons from MME sample 19XJ63-3 have more variable Ti contents of 1.51-78.8 ppm, which give variable temperatures between 620 and 1038°C. Temperature uncertainty is ± 4.5%. The Eu/Eu*, Zr/Hf, and Th/U ratios

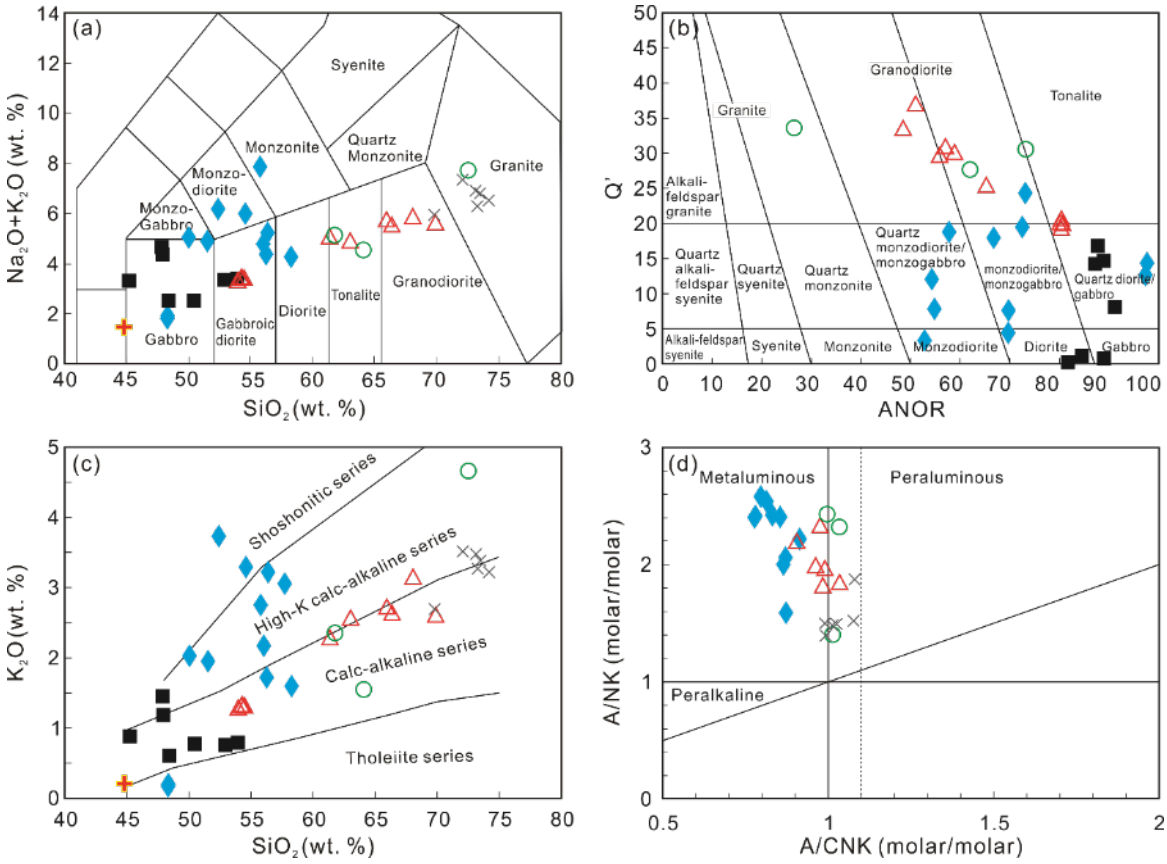

Figure 9. Whole-rock geochemical variations of the granitoids, MME, and mafic dyke from the TB and CP. (a) SiO_2 vs. $Na_2O + K_2O$ (TAS) diagram (*Le Maitre et al.,* 1989). (b) Q'-ANOR classification diagram (*Streckeisen & Le Maitre,* 1979). (c) SiO_2 vs. K_2O (wt%) classification diagram. (d) A/NK vs. A/CNK diagram. A/CNK = $Al_2O_3/(CaO + Na_2O + K_2O)$ in molar, A/NK = $Al_2O_3/(Na_2O + K_2O)$ in molar. The sample symbols are consistent with figure 6.

in 19XJ63-3 are positively correlated with Ti contents and accordingly the estimated T (Fig. 8d to f), suggesting fractionations with cooling (*Schmitt et al.,* 2017), whereas these relationships are more ambiguous for the host granodiorite (19XJ63-1). As for samples from the CP, the enclave (19XJ119-3) and host rock (19XJ119-1) show identical zircon compositions with nearly overlapped REE patterns. The restricted variations of Ti contents (6.5-12.2 ppm and 6.4-14.7 ppm, respectively) yield consistent temperatures of 707-765°C and 705-763°C. Both samples show nearly constant Eu/Eu* and Zr/Hf values within the limited temperature, which may support their rapid accumulation in a short time interval.

Titanite crystals from the host and enclave of the TB give similar REE patterns with positive LREE slope and relatively flat MREE-HREE slope (Fig. 8c). The high REE concentrations in the range of 2.61-4.38 wt% account for the large amount of REE in the whole rock. Their Zr contents range from 416 to 889 ppm. The high trace element contents, prominent negative Eu anomalies, high Th/U ratios as well as crystal shapes commonly indicate a magmatic origin. Meanwhile, similar crystal habit, size, and element compositions suggest possible crystal transfer between the host and enclave rocks, considering the lack of modal titanite in some granites.

4.3 Whole-rock geochemistry

4.3.1 Major and trace element

Because of the close spatial-temporal relationship, similar mineral compositions, and tectonic setting, we discuss the TB and CP together and only differentiate them when necessary. The host granitoids have SiO_2 contents ranging from 54.0 to 72.5 wt%, K_2O from 1.30 to 4.66 wt%, Na_2O from 2.04 to 3.75 wt%, and Al_2O_3 from 14.1 to 16.8 wt%, plotting into gabbroic diorite to granite in the TAS diagram (Fig. 9a), while mostly in the granodiorite range in the Q'-ANOR diagram (Fig. 9b). The high K_2O contents make them medium- to high-K calc-alkaline series (Fig. 9c), and they are metaluminous to weakly peraluminous with A/CNK all below 1.1 (Fig. 9d). They display relatively smooth compositional trends in the Harker diagrams (Fig. 10).

The mafic enclaves and dyke samples have low SiO_2 contents of 45.2-58.3 wt%. Variable K_2O (0.17-3.75 wt%) and Na_2O (1.63-5.09 wt%) contents make them plot into gabbro-diorite or monzogabbro-monzonite series in the TAS diagram (Fig. 9a) and tholeiite to shoshonitic series in the Si-K diagram (Fig. 9c). All of them are metaluminous with low A/CNK values (0.70-0.91; Fig. 9d). In the Harker diagrams (Fig. 10), there are big scatters in most major elements for these mafic rocks, which is attributed to either crystal accumulation or later stage modification and needs further explanations.

Regarding the trace elements, samples of the host granitoids from both TB and CP show relatively homogeneous compositions. They are characterized by variable V contents from 13 to 266 ppm, low Cr (0.2-77.2 ppm) and Ni (0.2-31.4 ppm) contents, and total REE of 91 to 187 ppm. The consistent REE patterns show LREE enrichment with $(La/Yb)_N$ ratios of 3.05 to 15.0 and flat HREE, with negative or positive Eu anomalies ($Eu/Eu^* = 0.66$-1.23; Fig. 11a and b). The enrichment in LILE and depletion in Nb, Ta, and Ti (Fig. 11c and d) suggest arc-like geochemistry, consistent with the syn-subduction generation. As for the MME and mafic dykes, some samples

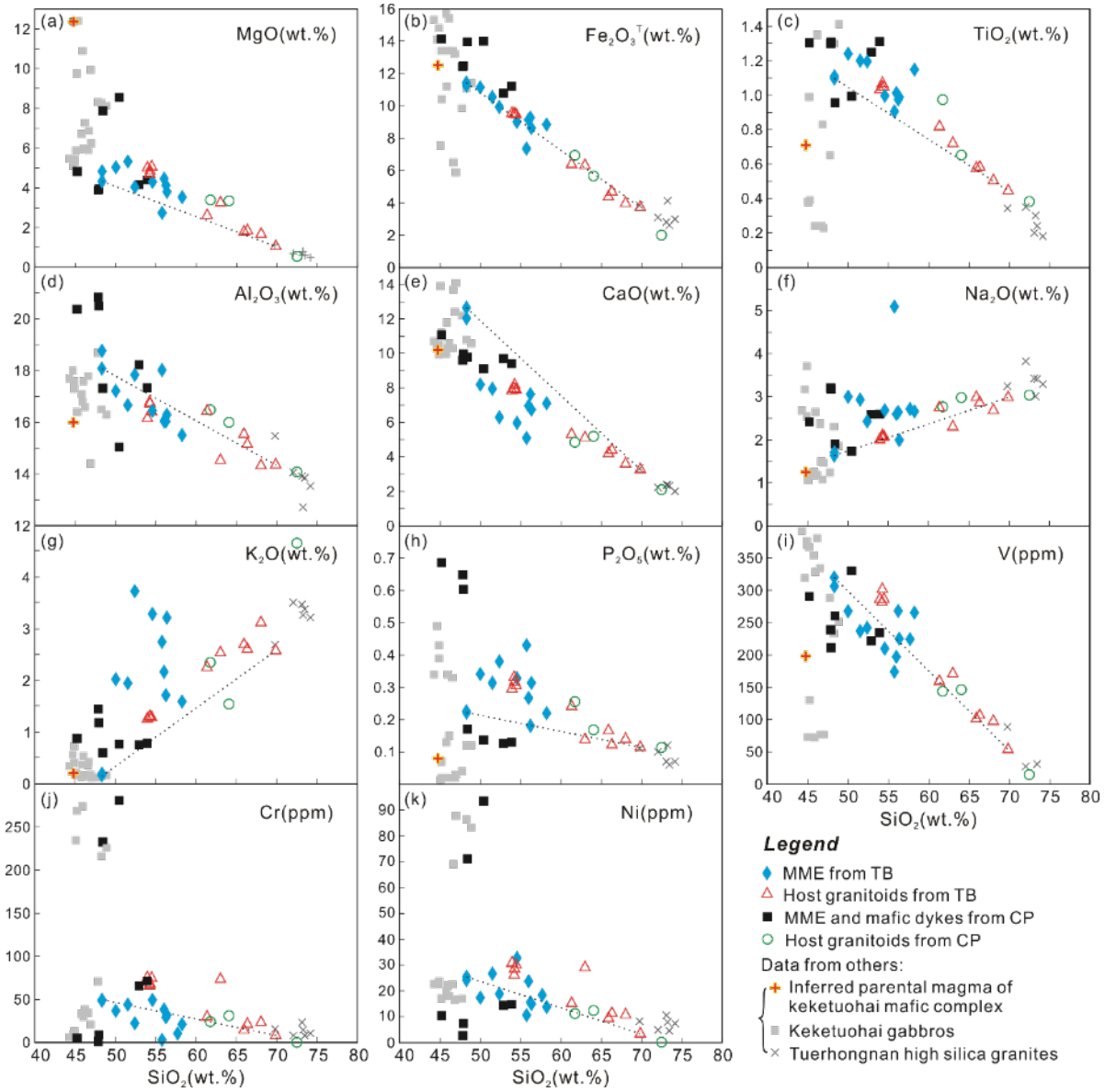

Figure 10. Harker diagrams for the granitoids, MME, and mafic dyke from the TB and CP.

show comparable REE concentrations with the host granitoids, together with similar LREE enrichment and flat HREE distribution patterns (Fig. 11a and b). Other samples, however, have much higher contents of REE (302-401 ppm), with variable LREE distribution ranging from the positive slope (19XJ63-4, 64-1, 64-2, 64-3, 69-2) through flat (19XJ119-3, 119-4, 119-5) to the negative slope

(19XJ63-3, 69-3). As shown in the spider diagrams (Fig. 11c and d), Nb, Ta, and Ti are also depleted for these mafic rocks, while the LILE, Th, and U are variably enriched or depleted.

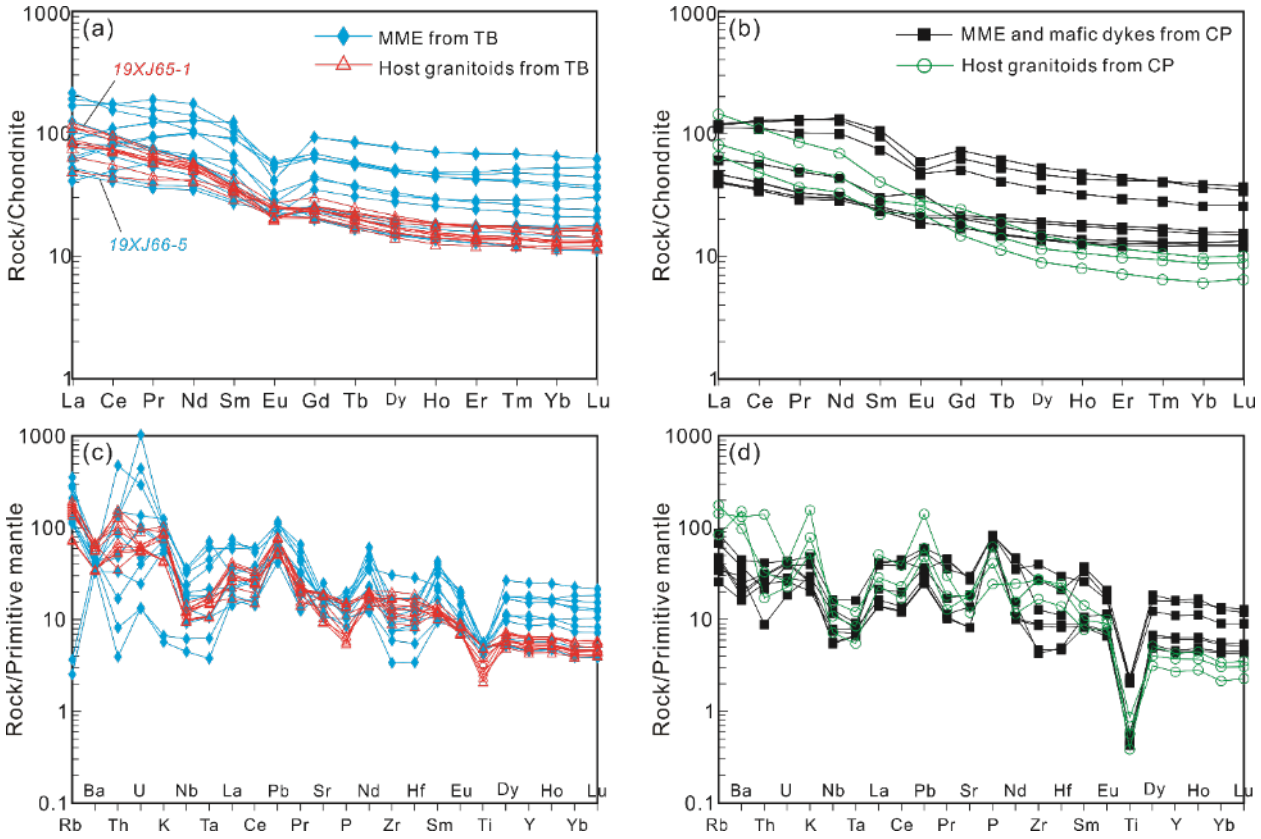

Figure 11. (a) (b) Chondrite-normalized REE patterns, and (c) (d) N-MORB-normalized trace element spider diagrams for the granitoids, MME, and mafic dyke from the TB and CP. The normalized values are from Sun & McDonough (1989).

4.3.1 Whole-rock Sr-Nd isotopes

Whole-rock Sr-Nd isotopic compositions for selected host granitoids and mafic enclaves from the TB and CP are shown in figure 12. The initial $^{87}Sr/^{86}Sr$ ratios are between 0.706274 and 0.715996, with the lowest for the mafic dyke (19XJ119-7) of the CP and the highest for a host granodiorite (19XJ65-1) of the TB. These two samples yield the highest and lowest Nd(t) values of +2.6 and -2.2, respectively, while other samples have near-chondrite Nd isotopic compositions with consistent Nd(t) of -0.5 to +0.5. The calculated two-stage Nd model ages are between 0.93 and 1.32 Ga, with an average value of ca. 1.13 Ga.

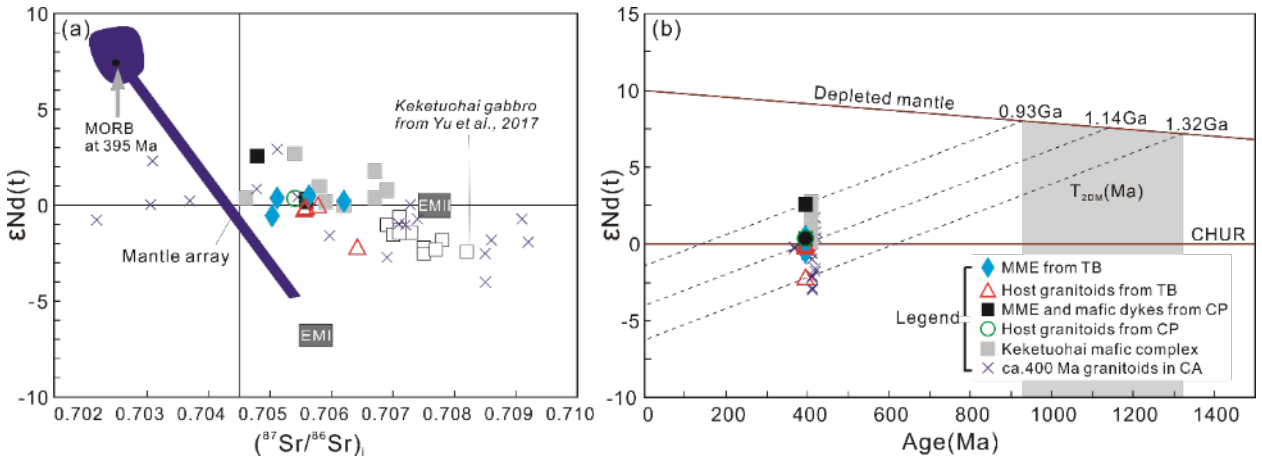

Figure 12. Whole-rock Sr-Nd isotopic compositions of the early Paleozoic mafic-felsic rocks from the Chinese Altai. (a) $(^{87}Sr/^{86}Sr)_i$ vs. Nd(t) diagram. (b) Nd(t) values vs. Age (Ma). Data sources are from *Cai et al.,* 2012, *Yu et al.,* 2017a, and *Cui et al.,* 2020.

4.4 Plagioclase in-situ Sr isotope

Sr isotopic analyses were performed on different positions of one single plagioclase phenocryst including core, mantle, and rim, and on plagioclase in the matrix. Overall, plagioclase throughout the TB shows relatively large variations in $(^{87}Sr/^{86}Sr)_i$ values between 0.7054 and 0.7089, with the highest value from sample 19XJ63-3. Plagioclase from the CP, in contrast, show limited variations in $(^{87}Sr/^{86}Sr)_i$ of 0.7053-0.7063. Given that some of the MME from the TB were severely altered, it is reasonable to infer that the very high values (above 0.7075) are due to local alteration by meteoric water, and are thus omitted for further discussion. From the analytical results, there is no systematic or regular variation in isotopic values of plagioclase in host rocks and enclaves, possibly due to the similarity or partial equilibrium of Sr isotopes between mafic and felsic magmas (Fig. 13). However, the large variations in the grain- or sub-grain scale suggest that the isotope system was not fully homogenized by diffusion but still preserve the magma source information. The intergranular changes of Sr isotopic composition, when combined with the plagioclase chemistry, has the capacity to trace the magmatic process.

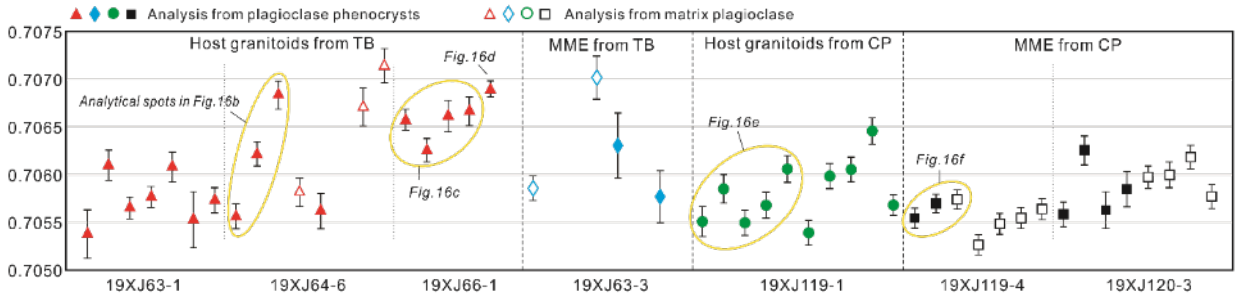

Figure 13. Plagioclase in-situ Sr isotopic compositions for the granitoids, MME, and mafic dyke from the TB and CP. Error bars are at 2 , and analytical results above 0.7075 are not shown in the diagram. Yellow circles are analytical spots shown in figure 16.

5 Discussion

5.1 Crystal accumulation and late-stage magmatic to sub-solidus alteration process

Crystal accumulation and late-stage alteration are common in our studied rocks, and these processes need to be first evaluated on account of their significant impact on whole-rock chemical compositions.

The crystal alignment and interlocking texture in some MME (19XJ119-3, 119-4, 119-5) from the CP indicate crystal accumulation (Fig. 3e). These enclaves are characterized by very low SiO_2 contents (45.2 – 47.9 wt%) inconsistent with their modal mineralogy (Fig. 9a). Their low Mg# of 43-45, low Cr and Ni, and high TiO_2, $Fe_2O_3{}^T$, Al_2O_3, P_2O_5, and Zr contents further suggest that they were not simply crystalized in basaltic liquids, but formed in more evolved liquids with accumulations of plagioclase, hornblende, apatite, Fe-Ti oxides, and zircon. The high abundance of REE is possibly a combined effect of apatite and hornblende accumulation (*Barbarin,* 2005).

The high water contents of many calc-alkaline magmas may result in late-stage chemical alteration. The abnormally high K_2O and Rb in the MME from the TB may be due to concentration of these elements in the newly formed or altered biotites, which is consistent with the presence of abundant biotite clots (Fig. 3a). High K_2O samples are simultaneously characterized by high abundances of REE and other incompatible elements such as Zr, Nb, Ta, etc. The distinctive LREE distribution patterns with positive slopes are compatible with those of the titanite (Fig. 8c and 11a), suggesting that fluids may have carried these elements and fix them into early formed accessory phases. Apatite is another important REE carrier, and the high P_2O_5 of some samples reflects their accumulation during phenocryst growth with local P_2O_5 saturation (*Hoskin et al.,* 2000). The abnormal enrichment of K_2O and some incompatible elements indicates that a hydrous and enriched melt at the final stage of granitic differentiation induced the auto-metasomatism of both enclave and host granite (*Bédard,* 1990). On the

other hand, the evidence for the effect of a hydrothermal fluid under sub-solidus condition comes from the ubiquity of epidote (Fig. 3), formed at ca. 300°C (*Parsapoor et al.,* 2015). Such hydrothermal alteration is also reflected by mild sericitization and/or clayization of some feldspar, appearance of actinolite (Fig. 6a), and re-equilibration of primary biotites (Fig. 6b). Therefore, samples from the TB variably suffered mineralogical and chemical modifications during the late-magmatic deuteric alteration to sub-solidus propylitization (*Féménias et al.,* 2006). Enclaves with relatively small volumes inevitably experienced more intense alteration (e.g., *Perugini et al.,* 2003), as suggested by their vastly scattered chemical compositions compared with more uniform ones of the host granitoids.

5.2 Magmatic processes in the deep source zone

5.2.1 The parental magma generation process

5.2.1.1 Host granitoids

Linear correlations for major and trace elements appear in the Harker diagrams for the host granitoids, which can be explained by fractional crystallization (FC) or assimilation-fractional crystallization (AFC) from more mafic magma, or magma mixing between mafic and felsic ones. Due to the lack of chilled margins of the mafic magma, we choose the most mafic gabbroic enclave (19XJ66-5) and the felsic granite (19XJ65-1) from the TB as two endmembers. The less alteration and accumulation character for this selected MME sample make it have a well-matched differentiation trend with the host granite. To distinguish the FC, AFC, and binary mixing, trace elements with high resistance to alteration were selected for elemental modeling using the PetroGram and partition coefficients therein (*Gündüz & Asan,* 2021), and the modeling results are shown in figure 14. The host granitoids generally fall on the magma mixing line, whereas crystallization from the mafic endmember with possible crustal assimilation cannot explain the compositional variations. The lack of country rock xenoliths and rarity of zircon xenocrysts, and relatively low whole-rock $^{87}Sr/^{86}Sr$ ratios also support that crustal assimilation was insignificant

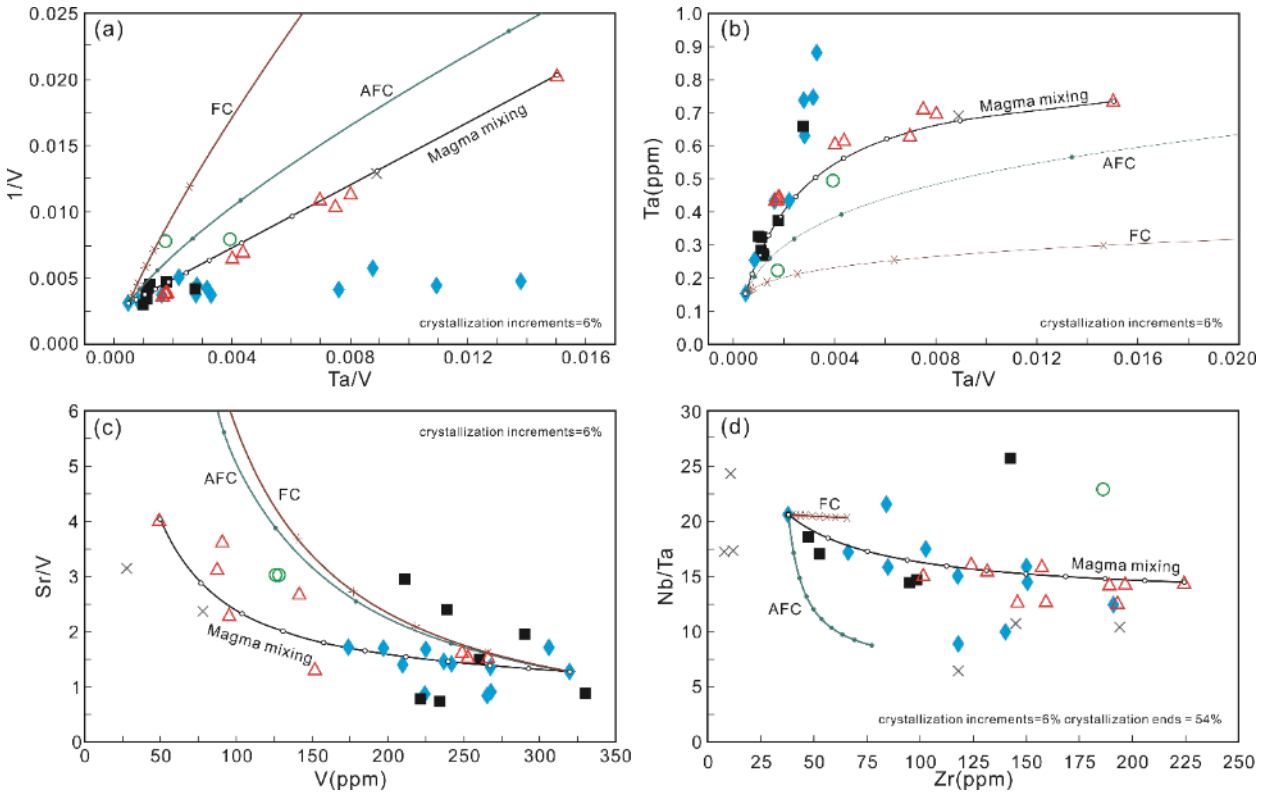

Figure 14. Trace element plots for the granitoids, MME, and mafic dyke from the TB and CP, showing models of fractional crystallization (FC), crustal assimilation and fractional crystallization (AFC), and magma mixing. The excel-based software PetroGram and method in the *Gündüz & Asan,* 2021 were applied. Gabbroic enclave 19XJ66-5 and host granite 19XJ65-1 were selected as the two endmembers for magma mixing, with ticks along the mixing curve show increments of 10% in the relative proportions. The FC and AFC trends were modelled based on the simplified mineral phase mode of 60 % plagioclase and 40 % amphibole, with whole-rock partition coefficients of D(V) = 4, D(Ta)= 0.276, D(Sr)=0.147, D(Nb)=0.294, and D(Zr)=0.295 for an intermediate melt. The ticks along the FC and AFC model curves show increments of 6% mass removal.

during the magma evolution. As shown in the REE pattern (Fig. 11a), the host granitoids have intermediate REE concentrations between the postulated two endmembers, which is in agreement with the mixing model. We further conducted a hybrid testing for the major elements using mass balance calculation following the method of *Fourcade and Allegre* (1981). Concentrations for each element in hybrid rocks should follow the expression: $C_H i = C_F i * X_F + C_M i * (1-X_F)$, and a straight line would form in the C_F-C_M vs. C_H-C_M diagram, whose slope gives the mass proportion of the mixture. As shown in figure 15, host

granitoids from the TB mostly fit a hypothetical mixing model with good linear correlations (R^2 close to unity), except for the quartz diorite sample 19XJ66-1

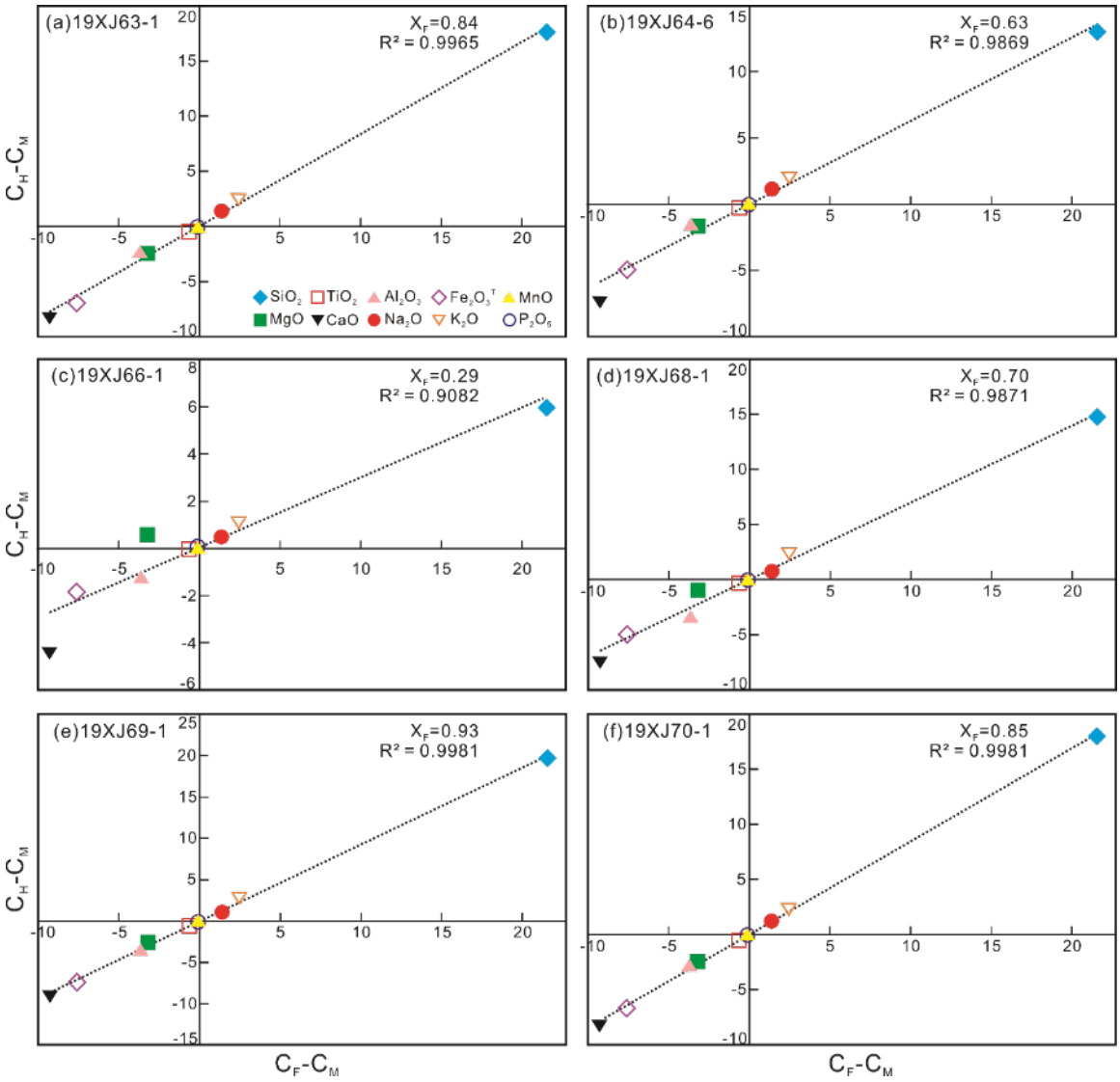

Figure 15. Major oxide mixing test for the hybrid host granitoids from the TB. Mass balance calculation follows the method in *Fourcade & Allegre,* 1981, using the same two end members (19XJ66-5 and 19XJ65-1) as those in figure 14. C_F, C_M, C_H respectively represent the elemental concentrations in felsic endmember, mafic endmember, and tested granitoids (hybrid rocks). X_F is the fraction of felsic endmember contribution. R represents the correlation coefficient.

(Fig. 15c), whose low correlations may be ascribed to some crystal accumulation

as inferred by its low SiO_2 and high P_2O_5 contents (Fig. 10).

Overall, combined major and trace element modeling strongly suggests that mixing between a mafic and a felsic magma is the most likely process accounting for the compositional trend displayed by the host granitoids and thus indicates a hybrid origin for their parental magma.

5.2.1.2 MME and mafic dyke

As discussed above, the petrographic characters indicates the igneous origins for the MME. The parental magma of these mafic rocks may represent either the differentiated product of pristine mantle-derived magma, or the hybrid product that is cogenetic with the granitoid (*Barbarin,* 2005; *Cheng et al.,* 2012; *Kumar & Rino,* 2006; *Perugini et al.,* 2003; *Turnbull et al.,* 2010; *R. Wiebe et al.,* 1997). Because of the strong interference of crystal accumulation and late-stage alteration, the chemical compositions of most studied mafic rocks do not represent the original liquids, so they did not have matched compositional trends in the elemental modeling (Fig. 14). Here we prefer the first explanation based on the evidence as follows. As discussed above, samples with high contents of Cr and Ni (19XJ120-3 and 120-4) may approximate the early liquids of the MME without evident accumulation. Their compositions are similar to the Keketuohai gabbros, whose parental magma was possibly differentiated from the primitive mantle-derived magma, leaving behind the cumulated Keketuohai mafic-ultramafic complex (*Cai et al.,* 2012). The high Cr and Ni values are hardly used as one endmember to account for the homogeneously low Cr-Ni values for other mafic rocks, whereas fractional crystallization could rapidly decrease their concentrations. Thus we infer that fractionation probably played the dominant role in the mafic magma evolution in the source region. Lack of any clinopyroxene crystal or relict in our enclaves or mafic dyke may suggest that the mafic magma had already evolved into a relatively mafic-intermediate composition in the deep source zone before ascending into the shallow level.

5.2.2 Sources of the mafic and felsic magmas

From analysis above, the host granitoids of the TB and CP were likely crystallized from the hybrid products of coeval mafic and felsic magmas, while the MME may represent either accumulates or quenched evolved mafic magmas. It is necessary to identify the two magmas with contrasting compositions.

Firstly, the most mafic sample (19XJ120-3) has evolved composition with low Mg# (59.9), which cannot represent mantle-equilibrated primary basaltic melt before earlier fractionation of olivine and pyroxene. The ca. 409 Ma Keketuohai mafic complex outcrops in the northern part of the TB, and the previous study suggested that the complex represents a set of magmatic series formed through fractional crystallization from an inferred high-Mg tholeiitic basaltic melt, which was derived from the SCLM that had been enriched by the previous subduction (*Cai et al.,* 2012; *Yu et al.,* 2017a). Our mafic rocks (enclaves and dyke) possess identical Nd(t) values to this complex (Fig. 12), and their proximity in time and space, similarities in mineral assemblages and chemical

compositions suggest a genetic correlation. Thus, we infer that the mafic magma likewise represents a differentiated component from partial melts of the SCLM. The host granitoid samples representing hybrid melts have Nd(t) values identical to or slightly lower than the mafic rocks (Fig. 12). It suggests that the felsic endmember during the hybridization should be isotopically similar to the mafic one, with near chondrite Nd isotopic compositions. The felsic magma thus may be either an advanced fractionation of cogenetic mantle-derived magma, or a low-degree partial melt of a relatively young and primitive lower crust of mantle derivation. Zircon Hf isotopic ratios are resistant to later stage alteration and crustal contamination and therefore provide information for the original magma composition from which zircons crystallized (*Kinny & Maas,* 2003). Despite some overlapping, the host granitoid from the TB (19XJ63-1) has overall more enriched zircon Hf isotopic ratios than the associated MME (19XJ64-2), confirming the existence of two isotopically different melts and precluding a simple origin by closed-system fractionation from a common mantle-derived magma (Fig. 5). Previous studies concluded that the widespread coeval granitic rocks in the Chinese Altai were produced by dehydration melting of the lower crust, which have similar isotopic compositions to our felsic samples and thus suggest the ubiquity of the primitive crustal melting (*Broussolle et al.,* 2019; *Cui et al.,* 2020; *Yu et al.,* 2017b; *Yuan et al.,* 2007). It is also consistent with the isotopic geochemical data for the highly metamorphosed rocks in the region, which indicate that the basement of the Chinese Altai is not made up of old crustal rocks but dominated by newly accreted materials (e.g., *Broussolle et al.,* 2019). Old continental blocks, however, exist in the western Mongolia and their erosion may supply detritus to the Chinese Altai (e.g., *Jiang et al.,* 2016), explaining the Precambrian ages of subordinate detrital zircons from the meta-sedimentary rocks. It is also the cause of somehow more enriched isotopic compositions for granitic rocks from the Chinese Altai, which enable the more felsic component for the precursor magmas to be identified.

5.2.3 The in-depth magma hybridization process

The interaction between different magmas is affected by many parameters, including relative volume and composition contrast of the two components, temperature, volatile content, and initial crystallinity of the magma (*Kumar & Rino,* 2006; *Snyder & Tait,* 1995). Based on the above discussion, we propose that the SCLM-derived mafic magma experienced differentiation and mixing with the juvenile crustal-derived felsic magma. This is a common process in a deep crustal hot zone (DCHZ in *Annen et al.,* 2006), where the mantle-derived magma ascends and ponds at the lower crust or crust/mantle boundary due to the high density. The high-T magma induces partial melting of the lower crust, which could be composed of older intrusions of cogenetic mantle-derived hydrous basalt or amphibolite, or unrelated pre-existing old metamorphic crustal rocks. In the DCHZ, the larger volumes of evolved mafic magmas, high-T, and high-H_2O conditions facilitate the magma mixing process. In the current study, the primitive magmas experienced fractional crystallization of mainly olivine, pyroxene, and possible amphibole, without garnet, suggesting a differentiation

depth shallower than the garnet-stable condition. The high Al_2O_3 in the residual basaltic magma indicate the restricted earlier fractionation of plagioclase, consistent with relatively high-H_2O condition. A juvenile mafic lower crust is inferred from the relatively depleted Nd and zircon Hf isotopic compositions as well as the respective model ages of the studied rocks. This study shows that hybrid melts were formed by mixing of the mafic magma with felsic one, which can detach and ascend into the shallow level due to the lower density, as represented by the host granitoid rocks of this study. A pulse of the residual mafic magma, in the meanwhile, could also ascend directly with less hybridization in depth, which is represented by the enclave/dyke magmas.

5.3 Evolution in the high-level magma reservoir

5.2.1 P-T-H_2O constraints

The crystallization pressures and thus the depth can be estimated using amphibole compositions. Al-in-amphibole geobarometer was established by *Anderson and Smith* (1995), for the appropriate buffering mineral assemblage of hornblende, plagioclase, biotite, orthoclase, quartz, Fe-Ti oxides, titanite, plus a vapor. The estimated pressures using this approach yield wide variations from 0.1 to 3.3 kbar, which may suggest that the actual mineral assemblage at the time of amphibole crystallization was different from *Anderson and Smith* (1995). On the other hand, a new thermobarometer of *Ridolfi et al.* (2010) was established for those amphiboles with a composition of Al-number 0.21 and Mg-number > 0.5, crystallized from calc-alkaline magmas. The primary magnesio-hornblende from our samples in compliance with the requirements are selected for calculation, which yield variable values of 1.0-2.2 kbar (Table S7-3) with equivalent depths of 3.5-7.7 km. It possibly implies a polybaric crystallization during the ascent of the magma (*Féménias et al.,* 2006).

Temperature estimation from amphibole compositions using equations of *Ridolfi et al.* (2010) gives consistent results of 818-837 °C, while the hornblende-plagioclase geothermometer of *Holland and Blundy* (1994) gives lower values between 666 to 789 °C. Zircon saturation temperatures reflect the minimum T for those inheritance-free, zircon-unsaturated melts before extensive crystallizations (*Miller et al.,* 2003), which yield 764-828 °C for the host granitoids, whereas those mafic rocks are out of the experimental calibration and give low values. Ti-in-zircon (*Fu et al.,* 2008) and Zr-in-titanite (*Hayden et al.,* 2007) thermometers give comparable averaged values at ca. 705-743 °C and 715-755 °C, respectively, suggesting a relatively late crystallization.

The widespread primary hornblende and biotite and absence of pyroxene suggest a hydrous magma for both the granitoids and enclaves. The primitive arc magma is originally H_2O-rich, generally confined in the range of 2-6 wt% (e.g., *Cervantes & Wallace,* 2003; *Müntener et al.,* 2001; *T. Sisson & Grove,* 1993). With differentiation in the deep source region, the water content increases and remains in the melt. Al-sensitive hygrometer of amphibole in *Ridolfi et al.* (2010) yields values between 5.8 and 7.7 wt% for the magnesio-hornblende from

individual samples with an accuracy of 0.4 wt% (Table S7-3), which suggests precipitation of the hornblende under water-saturated condition and records the minimum water contents at the onset of magma crystallization. Some water can be lost during further evolution, and the H_2O contents in the late stages of magma crystallization are typically estimated to be 4-6 wt% in calc-alkaline intermediate and silicic magmas (*Annen et al.,* 2006; *Jon Blundy & Cashman,* 2005).

A combination of P-T-H_2O estimation for studied rocks is provided in Table 1.

5.2.2 Magma hybridization at emplacement level: textural inferences

The rock texture and structure are mainly dominated by processes operated during and after the ascent and emplacement of magma batches into high-level magma chambers (*Jon Blundy & Cashman,* 2001). Some disequilibrium textural evidence in petrography reflects magma interaction during crystallization. Crystal size and shape are closely related to the interplay of nucleation and growth of crystals, which is then strongly controlled by magma undercooling, the depression of temperature below the equilibrium freezing temperature ($\Delta T = T_{liquids}\text{-}T_{magma}$). It has been suggested that large undercooling induces an increased nucleation rate, whereas small undercooling leads to an increased growth rate (*Vernon,* 2018). The needle-like apatite and bladed biotite are typical signs of rapid crystallization and are associated with high nucleation rates due to high ΔT, which suggests a quick thermal equilibration between the injected hot mafic magma and the felsic magma (*Baxter & Feely,* 2002; *Coombs et al.,* 2003). The large difference in mineral sizes shown in the transition zone between the enclave and host granite also supports a quick crystallization of the mafic magma (Fig. 3g and h). The interactive crystal transfer is evidenced by the penetration of some plagioclase phenocrysts from the host into the enclave side and the transfer of some titanite from the mafic to felsic magma.

5.2.3 Magma evolution and hybridization history: plagioclase records

5.2.3.1 Plagioclase characteristics

Plagioclase is a common mineral in mafic-felsic rocks, and the slow CaAl–NaSi diffusion and high resistance to high-T recrystallization allow plagioclase zoning to be well preserved, which can be used to monitor the long-lived magma evolution relating to the changing crystallization conditions (e.g., *Catherine Ginibre et al.,* 2002; *Grove et al.,* 1984; *Janoušek et al.,* 2000; *Janoušek et al.,* 2004; *Waight et al.,* 2000).

The composition and stability of the plagioclase is a function of melt composition and intensive parameters such as P, T, and H_2O (*Catherine Ginibre & Wörner,* 2007; *Putirka,* 2005; *Ruprecht & Wörner,* 2007; *Ustunisik et al.,* 2014). Plagioclase crystalized from the mafic magma tends to be more calcic with high An values (e.g., *Panjasawatwong et al.,* 1995). Experimental research has revealed that plagioclase An values are positively correlated with temperature and negatively with pressure. Thus, in a closed-system process, isobaric cooling results

in normally zoned plagioclase whereas decompression-driven crystallization induces reverse zoning, and convection of the magma caused by stirring in magma chamber could form the oscillatory zoning (*Catherine Ginibre et al.,* 2002; *Ustunisik et al.,* 2014). As confined by the experimental research in *Ustunisik et al.* (2014), the magnitude of the variation caused by pressure is relatively small on the order of 3% An per kbar. For the temperature, the cooling experiment from 1100 to 1000 °C at 1bar was accompanied by a 20 mol% decrease in An (An_{54}-An_{34}). The water content of the melt strongly controls the liquids and solidus for mineral phases, and an addition of 1.5 wt% water at 1 kbar and 1050 °C induces an increase of 30 mol% An content in the plagioclase. Experimental results from *Pichavant et al.* (2002) show that the plagioclase An values can reach as high as 80-90 in basaltic andesite and andesite melt under H_2O-saturated conditions (with up to 7-8 wt% H_2O) at 950 °C. On the other hand, in an open-system, magma recharge with different compositions may yield changes in both the physical condition and the chemical composition of the existing magma if mixing occurs, which will be reflected in the An values of plagioclase grown in the newly-equilibrated magma. Plagioclase An variations alone thus cannot distinguish between closed- and open-system behaviours. In-situ Sr isotope analysis of plagioclase has the ability to record inhomogeneity at grain- or sub-grain scale in relation to the open-system operations. For example, isotope heterogeneity in plagioclase can be caused by incomplete homogenization of various melt batches from heterogeneous or contrasting sources (e.g., *Braschi et al.,* 2014; *Ferrara et al.,* 1985; *C. Ginibre & Davidson,* 2014; *Karykowski et al.,* 2017; *Wilson et al.,* 2017). However, country rock assimilation and/or late-stage alteration can change the isotopic composition as well, which should be treated with caution. Therefore, a combination of morphological, chemical, and Sr isotopic characteristics of plagioclase was analyzed to provide implications for the recharge event in the magma chamber and the complete process of long-lived magma evolution (*Gagnevin et al.,* 2005; *C. Ginibre & Davidson,* 2014).

5.2.3.2 Plagioclase phenocryst profiles

As shown in figure 16a, the phenocryst from 19XJ64-6 displays clear zonation as reflected by the brightness of interference color. A bright core with a curving resorption surface is bordered by a dark zone 200 m wide, then a very thin bright zone, and finally a euhedral dark rim. Compositional profile from A_1 to B_1 reveals that the brightness zonation correlates well with the An value. The high An value of the plagioclase core (ca. 80) indicates equilibrium with a high-

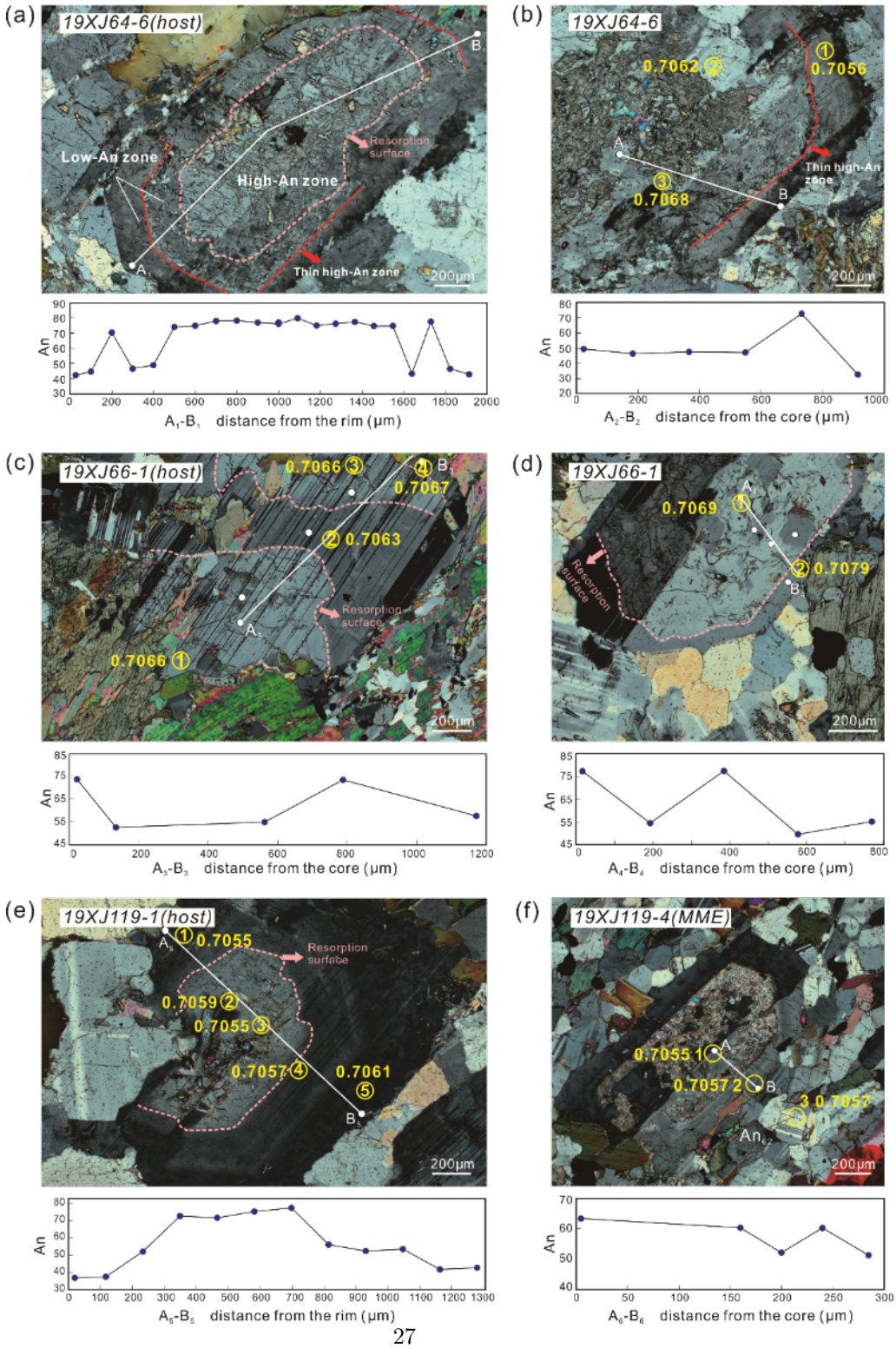
(a)
19XJ64-6(host)
Low-An zone
High-An zone
Resorption surface
Thin high-An zone
200μm
An
A1-B1 distance from the rim (μm)
(b)
19XJ64-6
0.7062 ②
① 0.7056
③ 0.7068
Thin high-An zone
200μm
An
A2-B2 distance from the core (μm)
(c)
19XJ66-1(host)
0.7066 ③
④ 0.7067
② 0.7063
Resorption surface
0.7066 ①
200μm
An
A3-B3 distance from the core (μm)
(d)
19XJ66-1
0.7069 ①
② 0.7079
Resorption surface
200μm
An
A4-B4 distance from the core (μm)
(e)
19XJ119-1(host)
① 0.7055
Resorption surface
0.7059 ②
0.7055 ③
0.7057 ④
0.7061 ⑤
200μm
An
A5-B5 distance from the rim (μm)
(f)
19XJ119-4(MME)
0.7055 1
0.7057 2
3 0.7057
An62
200μm
An
A6-B6 distance from the core (μm)

Figure 16. Cross-polarized light photomicrographs, An value profiles, and in-situ Sr isotopic compositions of the plagioclase phenocrysts from host granitoids of the TB (a-d) and CP (e), and MME form the CP (f). White circles in the phenocrysts are locations of EPMA analysis. Yellow circles and numbers are Sr isotope analytical spots and results.

H_2O melt. The sharp decrease of An (An_{80}-An_{46}) to the mantle cannot be explained by the changing P or T, as it is impossible to have such a big pressure increase in the high-level magma chamber or temperature decrease for the large volume of host granitic magma. Instead, it may reflect a degassing-induced crystallization that commonly occurs in the rapid ascent with decompression, especially for those magmas with high volatile contents and moderate melt viscosities (e.g., *Annen et al.,* 2006; *Jon Blundy & Cashman,* 2001; *Cashman & Blundy,* 2000; *Crabtree & Lange,* 2011). Then the very thin calcic ring with An spike most likely reflects an impinge of another pulse of mafic magma, during which the combination of increased T and H_2O and possible local melt mixing affected the plagioclase composition. The thin high-An zone is immediately followed by a low An rim equilibrated with the final host magma, possibly due to quick chemical and thermal equilibrium concerning the very low relative abundance of mafic to felsic magma. This scenario is manifested in another big phenocryst from this sample (Fig. 16b). In this plagioclase, the high-An core (ca. 80) is absent and replaced by An_{50} that corresponds to the mantle region of the former phenocryst, suggesting that it started to crystallize at the second stage after degassing. The relatively low initial $^{87}Sr/^{86}Sr$ ratio in the rim may represent the isotope equilibration after mixing with a low $^{87}Sr/^{86}Sr$ mafic magma due to the fast diffusion of Sr isotope (e.g., *Lesher,* 1990; *Poli et al.,* 1996).

Figures 16c and d show phenocrysts from 19XJ66-1. Analytical spots were selected respectively from the bright and dark zones shown in the microphotographs, and the measured An contents correspond to high and low values. Unlike sample 19XJ64-6, these two phenocrysts lack regular zonation but have spot-like or irregularly corroded fillings surrounded by a dark rim. This phenomenon is also consistent with a decompression-degassing process, during which the resorbed high-An plagioclase was followed by more sodic plagioclase, which was newly precipitated and stable in a low-P and low-H_2O condition. Although no An spikes are discovered, the low $(^{87}Sr/^{86}Sr)_i$ values in the dark zone (Fig. 16c) possibly reflect some mafic magma assimilation during the second-stage crystallization. The distinctly high isotopic values in the rim (Fig. 16d), however, may represent a late-stage alteration.

With regard to the CP, a similar explanation for the two populations of An values can be applied to the phenocryst from granite 19XJ119-1 (Fig. 16e), where low An mantle surrounds the high-An inner core, and the rim with the lowest An is related to the sub-solidus process. The general core-rim texture of the phenocryst from the enclave sample 19XJ119-4 is manifested by a calcic core with more intense alteration and a rim characterized by alternating high- and

low-An values (Fig. 16f). The high An core (as high as 90) is considered to have crystallized from a hydrous mafic magma prior to its injection into the acidic magma chamber (*Browne et al.,* 2006). The variable An in the narrow rim may result from degassing, convection, cooling, and successive assimilation with the felsic host magma. The fine-grained matrix possibly marked the fast cooling of the enclave magma upon intruding into a relatively low-T felsic magma. Because the chemical exchange is not as efficient as the thermal equilibration, the matrix records two populations of the An values (e.g., 53 and 62), with the lower one recording the equilibrium with locally mixed melt during the crystallization history of the enclave magma.

5.2.3 Ascent and crystallization path accompanied by magma hybridization

The P-T-t path followed by individual magma batches controls the resulting phase assemblage, chemistry, and texture. We here put forward the possible crystallization path of the granitoid and enclave magma after extraction from the source zone based on the existing data from mineral chemistry, morphology, and isotopic data. The hydrous parental magma possibly ascended near adiabatically into the shallow level due to the low density and viscosity (*Annen et al.,* 2006), where the decompression of a water-saturated melt inevitably induced degassing with decreased capacity of accommodating volatile at ~~in~~ lower pressure. When the melt intersected the water-saturated liquids, it started to crystallize amphibole and/or plagioclase as the liquidus phase according to the chemical compositions. As calculated for the amphibole-bearing rocks, the relatively high-P of ca. 2.2 kbar and high H_2O of ca. 7.2-7.7 wt% limit the minimum initial crystallization condition. As illustrated by the widely developed core-rim texture of plagioclase phenocrysts from both the granitoids and MME, two populations of An values were yielded, with phenocryst cores having the highest An and the matrix plotting at the sodic end of the phenocryst mantle or rim. The relatively large cores (An~80-90) should be homogeneously formed in the early high-H_2O and high-P stage, in which condition the small undercooling (low ΔT) resulted in a high growth rate. The crystal-carrying magma ascended further into the final emplacement level with continuous degassing, which is recorded by the variable pressure and water content estimations from amphibole (Table 1). The low-P estimates of ca. 1.0-1.2 kbar roughly constrain the emplacement depth at or shallower than ca. 4 km. At this moment, the large undercooling caused by degassing and moderate cooling changed the crystallization model from growth-controlled to nucleation-controlled (*Vernon,* 2018), which is compatible with the sodic mantle-rim overgrown and small, unzoned plagioclase of matching composition in the groundmass. Increasing crystals increased the viscosity of the magma and finally limited its further ascent.

For the host granitoid, it was locally disturbed by mafic input during the emplacement, and only a few plagioclase phenocrysts recorded such a replenishment event by increased An content as shown in figures 16a and b. However, the relatively large variation in the plagioclase Sr isotopes between two possible end members do indicate the disturbance of the mafic magma and isotope diffusion.

For the MME, in addition to the effect of decompression upon ascent, the rapid heat loss of the enclave magma to the enclosing granite magma resulted in a larger undercooling, with needle-like apatite and tiny matrix crystals formed. Further processing in the shallow magma chamber, including more advanced fractional crystallization, may take place in tandem with crystal transfer and chemical mixing/assimilation with host magma, making it compositionally grading toward the felsic end.

Therefore, during the magma interaction at the shallow level, thermal equilibration and isotope exchange were relatively efficient between the mixing melts. Especially for samples from the CP, the smaller variation of Sr isotopic data, combining with the comparable zircon Hf(t) values and overlapped zircon trace element compositions, suggests a more thorough re-equilibration. Meanwhile, the partial chemical equilibration is reflected by the similarity in mineral compositions but heterogeneity in major elements. Therefore, mingling and local mixing occurred between each blob of mafic magma and the enclosing granitoid magma during crystallization in the high-level chamber, which differed from the thorough mixing at depth.

5 Conclusions

The TB and CP represent discrete portions active in the subduction stage of the Chinese Altai and can be typified as the calc-alkaline arc-related intrusions. By describing magmatic and subsolidus processes in the deep and shallower magma reservoirs, we could have a general model for the full evolutionary path of the studied granitoids and associated mafic rocks (Fig. 17), involving mafic-felsic magma interplay and other magmatic processes, in deep and shallow chambers, respectively.

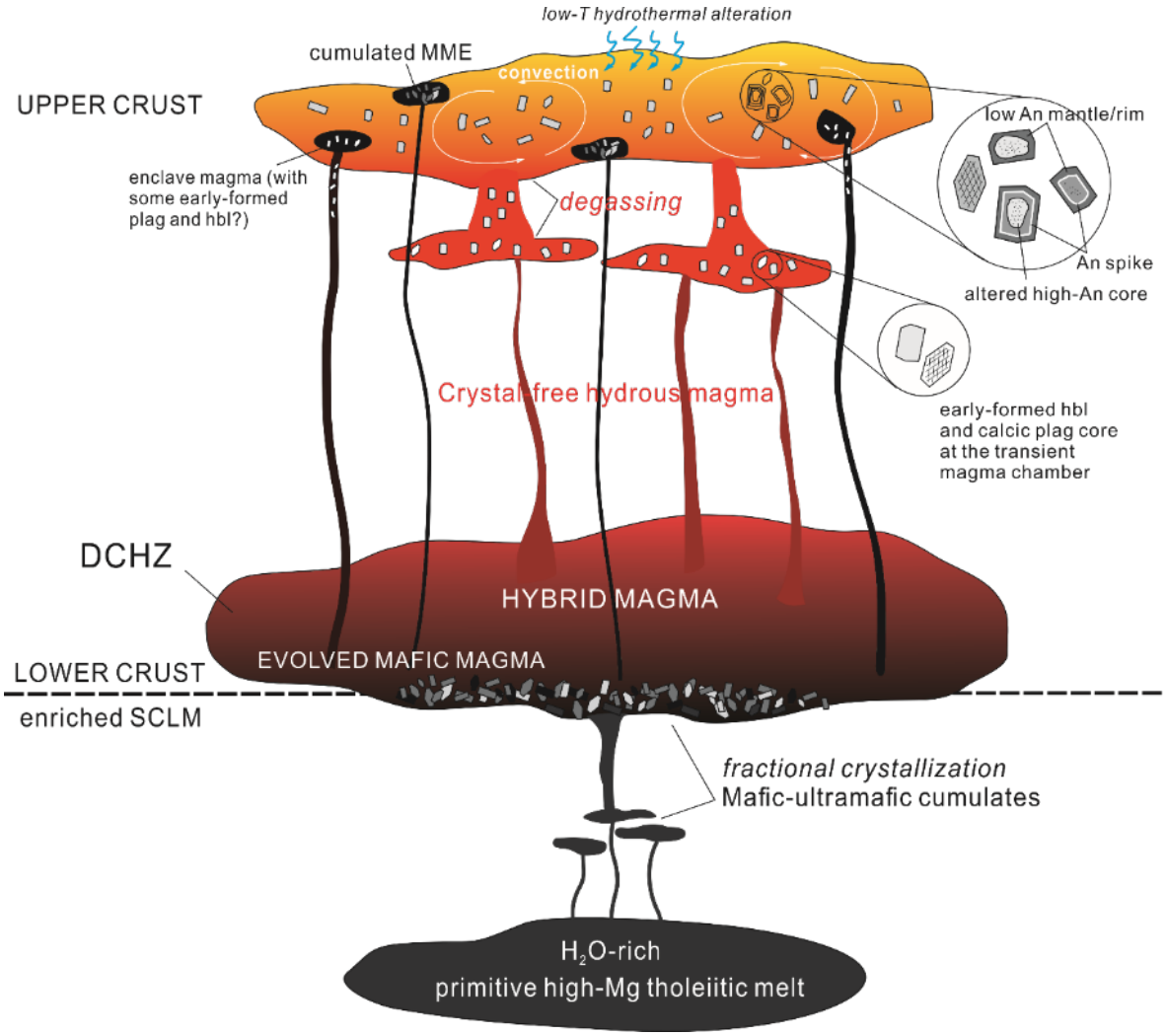

Figure 17. Schematic diagram showing the generation and evolution of the TB and CP in the Chinese Altai, involving magma generation, hybridization in the DCHZ, magma ascent and crystallization in shallow level, and late-stage alteration. See text descriptions in conclusion for the complete scenario.

(1) The SCLM was variably enriched by the slab fluid or melt during the long-lived subduction of the paleo-Asian ocean, leaving an enriched isotopic composition. High-Mg tholeiitic magma generated by partial melting of the SCLM underplated and ponded at the base of the arc crust, where it experienced extensive crystallization accumulation. The hot mafic magma induced partial melting of the existing juvenile crustal rocks. Under the high-T and hydrous condition, the evolved residual basaltic magma and the crustal-derived felsic magma could extensively mix to form the hybrid magma in the DCHZ.

(2) Due to the relatively low viscosity and density, the hybrid magma with varying mixture proportions may segregate and ascend near adiabatically to the upper crustal level, forming the granitic magma chamber. The rarity of inherited-zircons suggests a nearly crystal-free ascending path, and the fully molten state of the magma is a consequence of high water content. The very calcic cores of some plagioclase phenocrysts (An~80) mark the onset of crystallization at high pH_2O condition (at ca. 7 km). After stalling at this level briefly, the further ascent at the emplacement level marked the second-stage crystallization, which was accompanied by H_2O exsolution. The low-An rim of the plagioclase phenocrysts and matrix plagioclase suggest crystallization at this shallower level.

(3) Some evolving residual basaltic magma with little interaction with felsic magma also had chances to ascend in response to possible local stress relaxation. It episodically intruded into the incompletely crystallized felsic chamber, carrying some amphibole and calcic plagioclase (An as high as 90) crystallized at relatively deeper depth from the hydrous mafic-intermediate melt. Upon injection, the magma experienced further crystal fractionation and accumulation at the floor or wall of the chamber with the magmatic flow. Some of the enclaves represent cumulates while others were crystallized from the liquids during rapid cooling below solidus with fine-grained textures. Interactions between host and enclave magmas at the emplacement level were manifested in crystal transfer, thermal equilibrium, isotope diffusion, and to a less extent, chemical exchange. The volumetrically small mafic magma was more easily assimilated by the host magma during its crystallization or chilling process, while only a portion of host magma locally recorded the mafic disturbance by the chemical and/or isotopic compositions of crystallizing minerals. Further replenishment of the mafic melts into a sufficiently cooled magma chamber formed the cross-cutting mafic dyke, which had very limited interaction with the felsic magma in the form of minor crystal transfer (Fig. 3f).

(4) The mafic enclaves in the calc-alkaline batholiths, especially for the TB, experienced extensive deuteric alteration by the late-stage residual melt with high water and trace element contents. The alteration lasted to a lower temperature after the solidification of the rocks, and such sub-solidus alteration was widespread due to the very shallow level of the emplacement for both the TB and CP, which induced mineral alteration and formed some new phases such as epidote, sericite, and clay minerals.

Acknowledgments, Samples, and Data

This work was financially supported by Hong Kong RGC GRF (17302317 and 17303415), National Key R&D Program of China (2017YFC0601205), NSFC Projects (41730213, 42072264, 41902229, and 41972237), and the International Partnership Program of Chinese Academy of Sciences (Grant No.132744KYSB20190039). We are uploading the dataset to the EarthChem Library data repository and data archiving is underway. A copy of data is also uploaded as Supporting Information for review purposes. This is a contribution

of the Joint Laboratory of Chemical Geodynamics between The University of Hong Kong and Guangzhou Institute of Geochemistry, Chinese Academy of Science. We thank Mr. Zhou Ningchao from the Xi'an Geological Survey Center of China Geological Survey for the EPMA experiment assistance, and all members of the Wuhan Sample Solution Analytical Technology Co., Ltd and Nanjing FocuMS Technology Co. Ltd for other experimental assistance.

References

Anderson, J. L., & Smith, D. R. (1995). The effects of temperature and fO on the Al-in-hornblende barometer. *American Mineralogist, 80*(5-6), 549-559. doi:10.2138/am-1995-5-615

Annen, C., Blundy, J. D., & Sparks, R. S. J. (2006). The Genesis of Intermediate and Silicic Magmas in Deep Crustal Hot Zones. *JOURNAL OF PETROLOGY, 47*(3), 505-539. doi:10.1093/petrology/egi084

Barbarin, B. (2005). Mafic magmatic enclaves and mafic rocks associated with some granitoids of the central Sierra Nevada batholith, California: nature, origin, and relations with the hosts. *Lithos, 80*(1-4), 155-177. doi:10.1016/j.lithos.2004.05.010

Baxter, S., & Feely, M. (2002). Magma mixing and mingling textures in granitoids: examples from the Galway Granite, Connemara, Ireland. *Mineralogy and Petrology, 76*(1-2), 63-74. doi:10.1007/s007100200032

Bédard, J. (1990). Enclaves from the A-type granite of the Mégantic Complex, White Mountain Magma Series: Clues to granite magmagenesis. *Journal of Geophysical Research: Solid Earth, 95*(B11), 17797-17819. doi:10.1029/JB095iB11p17797

Blundy, J., & Cashman, K. (2001). Ascent-driven crystallisation of dacite magmas at Mount St Helens, 1980–1986. *Contributions to Mineralogy and Petrology, 140*(6), 631-650. doi:10.1007/s004100000219

Blundy, J., & Cashman, K. (2005). Rapid decompression-driven crystallization recorded by melt inclusions from Mount St. Helens volcano. *Geology, 33*(10), 793-796. doi:doi.org/10.1130/G21668.1

Blundy, J., & Sparks, R. (1992). Petrogenesis of mafic inclusions in granitoids of the Adamello Massif, Italy. *JOURNAL OF PETROLOGY, 33*(5), 1039-1104.

Braschi, E., Francalanci, L., Tommasini, S., & Vougioukalakis, G. E. (2014). Unraveling the hidden origin and migration of plagioclase phenocrysts by in situ Sr isotopes: the case of final dome activity at Nisyros volcano, Greece. *Contributions to Mineralogy and Petrology, 167*(3). doi:10.1007/s00410-014-0988-4

Broussolle, A., Aguilar, C., Sun, M., Schulmann, K., Štípská, P., Jiang, Y., et al. (2018). Polycyclic Palaeozoic evolution of accretionary orogenic wedge in

the southern Chinese Altai: Evidence from structural relationships and U–Pb geochronology. *Lithos, 314*, 400-424. doi:10.1016/j.lithos.2018.06.005

Broussolle, A., Sun, M., Schulmann, K., Guy, A., Aguilar, C., Štípská, P., et al. (2019). Are the Chinese Altai "terranes" the result of juxtaposition of different crustal levels during Late Devonian and Permian orogenesis? *Gondwana Research, 66*, 183-206. doi:10.1016/j.gr.2018.11.003

Brown, E., & McClelland, W. (2000). Pluton emplacement by sheeting and vertical ballooning in part of the southeast Coast Plutonic Complex, British Columbia. *Geological Society of America Bulletin, 112*(5), 708-719. doi:10.1130/0016-7606(2000)112<708:PEBSAV>2.0.CO;2

Browne, B. L., Eichelberger, J. C., Patino, L. C., Vogel, T. A., Dehn, J., Uto, K., et al. (2006). Generation of Porphyritic and Equigranular Mafic Enclaves During Magma Recharge Events at Unzen Volcano, Japan. *JOURNAL OF PETROLOGY, 47*(2), 301-328. doi:10.1093/petrology/egi076

Cai, K., Sun, M., Yuan, C., Zhao, G., Xiao, W., & Long, X. (2012). Keketuohai mafic–ultramafic complex in the Chinese Altai, NW China: petrogenesis and geodynamic significance. *Chemical Geology, 294*, 26-41. doi:10.1016/j.chemgeo.2011.11.031

Cai, K., Sun, M., Yuan, C., Zhao, G., Xiao, W., Long, X., et al. (2011). Prolonged magmatism, juvenile nature and tectonic evolution of the Chinese Altai, NW China: Evidence from zircon U–Pb and Hf isotopic study of Paleozoic granitoids. *Journal of Asian Earth Sciences, 42*(5), 949-968. doi:10.1016/j.jseaes.2010.11.020

Cashman, K., & Blundy, J. (2000). Degassing and crystallization of ascending andesite and dacite. *Philosophical Transactions of the Royal Society of London. Series A: Mathematical, Physical and Engineering Sciences, 358*(1770), 1487-1513. doi:10.1098/rsta.2000.0600

Castro, A., Gerya, T., Garcia-Casco, A., Fernandez, C., Diaz-Alvarado, J., Moreno-Ventas, I., et al. (2010). Melting Relations of MORB-Sediment Melanges in Underplated Mantle Wedge Plumes; Implications for the Origin of Cordilleran-type Batholiths. *JOURNAL OF PETROLOGY, 51*(6), 1267-1295. doi:10.1093/petrology/egq019

Cervantes, P., & Wallace, P. J. (2003). Role of H2O in subduction-zone magmatism: new insights from melt inclusions in high-Mg basalts from central Mexico. *Geology, 31*(3), 235-238. doi:10.1130/0091-7613(2003)031<0235:ROHOIS>2.0.CO;2

Chappell, B. (1996). Magma mixing and the production of compositional variation within granite suites: evidence from the granites of southeastern Australia. *JOURNAL OF PETROLOGY, 37*(3), 449-470. doi:10.1093/petrology/37.3.449

Chappell, B. W., White, A., & Wyborn, D. (1987). The importance of residual source material (restite) in granite petrogenesis. *JOURNAL OF PETROLOGY, 28*(6), 1111-1138. doi:10.1093/petrology/28.6.1111

Chappell, B. W., & White, A. J. (2001). Two contrasting granite types: 25 years later. *Australian Journal of Earth Sciences, 48*(4), 489-499. doi:10.1046/j.1440-0952.2001.00882.x

Cheng, Y., Spandler, C., Mao, J., & Rusk, B. G. (2012). Granite, gabbro and mafic microgranular enclaves in the Gejiu area, Yunnan Province, China: a case of two-stage mixing of crust- and mantle-derived magmas. *Contributions to Mineralogy and Petrology, 164*(4), 659-676. doi:10.1007/s00410-012-0766-0

Coleman, D. S., Gray, W., & Glazner, A. F. (2004). Rethinking the emplacement and evolution of zoned plutons: Geochronologic evidence for incremental assembly of the Tuolumne Intrusive Suite, California. *Geology, 32*(5), 433-436. doi:10.1130/G20220.1

Coombs, M. L., Eichelberger, J. C., & Rutherford, M. J. (2003). Experimental and textural constraints on mafic enclave formation in volcanic rocks. *Journal of Volcanology and Geothermal Research, 119*(1-4), 125-144. doi:10.1016/S0377-0273(02)00309-8

Crabtree, S. M., & Lange, R. A. (2011). Complex Phenocryst Textures and Zoning Patterns in Andesites and Dacites: Evidence of Degassing-Induced Rapid Crystallization? *JOURNAL OF PETROLOGY, 52*(1), 3-38. doi:10.1093/petrology/egq067

Cui, X., Sun, M., Zhao, G., Zhang, Y., Yao, J., & Han, Y. (2020). Geochronological and geochemical study of the high-grade orthogneissic rocks from the Northern Fuyun Complex: Implications for crustal architecture and Early-Middle Paleozoic evolution of the Chinese Altai. *Lithos, 366-367*. doi:10.1016/j.lithos.2020.105547

DORAIS, M. J., WHITNEY, J. A., & RODEN, M. F. (1990). Origin of mafic enclaves in the Dinkey Creek pluton, central Sierra Nevada batholith, California. *JOURNAL OF PETROLOGY, 31*(4), 853-881.

Féménias, O., Mercier, J.-C. C., Nkono, C., Diot, H., Berza, T., Tatu, M., et al. (2006). Calcic amphibole growth and compositions in calc-alkaline magmas: Evidence from the Motru Dike Swarm (Southern Carpathians, Romania). *American Mineralogist, 91*(1), 73-81. doi:10.2138/am.2006.1869

Ferrara, G., Laurenzi, M., Taylor Jr, H., Tonarini, S., & Turi, B. (1985). Oxygen and strontium isotope studies of K-rich volcanic rocks from the Alban Hills, Italy. *Earth and Planetary Science Letters, 75*(1), 13-28. doi:10.1016/0012-821X(85)90046-9

Ferry, J. M., & Watson, E. B. (2007). New thermodynamic models and revised calibrations for the Ti-in-zircon and Zr-in-rutile thermometers. *Contributions to Mineralogy and Petrology, 154*(4), 429-437. doi:10.1007/s00410-007-0201-0

Fourcade, S., & Allegre, C. J. (1981). Trace elements behavior in granite genesis: A case study The calc-alkaline plutonic association from the Querigut complex

(Pyrénées, France). *Contributions to Mineralogy and Petrology, 76*(2), 177-195. doi:10.1007/BF00371958

Fu, B., Page, F. Z., Cavosie, A. J., Fournelle, J., Kita, N. T., Lackey, J. S., et al. (2008). Ti-in-zircon thermometry: applications and limitations. *Contributions to Mineralogy and Petrology, 156*(2), 197-215. doi:10.1007/s00410-008-0281-5

Gagnevin, D., Daly, J., Poli, G., & Morgan, D. (2005). Microchemical and Sr isotopic investigation of zoned K-feldspar megacrysts: insights into the petrogenesis of a granitic system and disequilibrium crystal growth. *JOURNAL OF PETROLOGY, 46*(8), 1689-1724. doi:10.1093/petrology/egi031

Gehrels, G., Rusmore, M., Woodsworth, G., Crawford, M., Andronicos, C., Hollister, L., et al. (2009). U-Th-Pb geochronology of the Coast Mountains batholith in north-coastal British Columbia: Constraints on age and tectonic evolution. *Geological Society of America Bulletin, 121*(9-10), 1341-1361. doi:10.1130/B26404.1

Ginibre, C., & Davidson, J. P. (2014). Sr Isotope Zoning in Plagioclase from Parinacota Volcano (Northern Chile): Quantifying Magma Mixing and Crustal Contamination. *JOURNAL OF PETROLOGY, 55*(6), 1203-1238. doi:10.1093/petrology/egu023

Ginibre, C., & Wörner, G. (2007). Variable parent magmas and recharge regimes of the Parinacota magma system (N. Chile) revealed by Fe, Mg and Sr zoning in plagioclase. *Lithos, 98*(1-4), 118-140. doi:10.1016/j.lithos.2007.03.004

Ginibre, C., Wörner, G., & Kronz, A. (2002). Minor-and trace-element zoning in plagioclase: implications for magma chamber processes at Parinacota volcano, northern Chile. *Contributions to Mineralogy and Petrology, 143*(3), 300-315. doi:10.1007/s00410-002-0351-z

Grove, T. L., Baker, M. B., & Kinzler, R. J. (1984). Coupled CaAl-NaSi diffusion in plagioclase feldspar: experiments and applications to cooling rate speedometry. *Geochimica et Cosmochimica Acta, 48*(10), 2113-2121. doi:10.1016/0016-7037(84)90391-0

Grove, T. L., Elkins-Tanton, L. T., Parman, S. W., Chatterjee, N., Müntener, O., & Gaetani, G. A. (2003). Fractional crystallization and mantle-melting controls on calc-alkaline differentiation trends. *Contributions to Mineralogy and Petrology, 145*(5), 515-533. doi:10.1007/s00410-003-0448-z

Gündüz, M., & Asan, K. (2021). PetroGram: An excel-based petrology program for modeling of magmatic processes. *Geoscience Frontiers, 12*(1), 81-92. doi:10.1016/j.gsf.2020.06.010

Hayden, L. A., Watson, E. B., & Wark, D. A. (2007). A thermobarometer for sphene (titanite). *Contributions to Mineralogy and Petrology, 155*(4), 529-540. doi:10.1007/s00410-007-0256-y

Holland, T., & Blundy, J. (1994). Non-ideal interactions in calcic amphiboles

and their bearing on amphibole-plagioclase thermometry. *Contributions to Mineralogy and Petrology, 116*(4), 433-447.

Hoskin, P. W., Kinny, P. D., Wyborn, D., & Chappell, B. W. (2000). Identifying accessory mineral saturation during differentiation in granitoid magmas: an integrated approach. *JOURNAL OF PETROLOGY, 41*(9), 1365-1396. doi:10.1093/petrology/41.9.1365

Idrus, A. (2018). Petrography and Mineral Chemistry of Magmatic and Hydrothermal Biotite in Porphyry Copper-Gold Deposits: A Tool for Understanding Mineralizing Fluid Compositional Changes During Alteration Processes. *Indonesian Journal on Geoscience, 5*(1). doi:10.17014/ijog.5.1.47-64

Janoušek, V., Bowes, D., Braithwaite, C. J., & Rogers, G. (2000). Microstructural and mineralogical evidence for limited involvement of magma mixing in the petrogenesis of a Hercynian high-K calc-alkaline intrusion: the Kozárovice granodiorite, Central Bohemian Pluton, Czech Republic. *TRANSACTIONS-ROYAL SOCIETY OF EDINBURGH, 91*(1/2), 15-26. doi:10.1017/S0263593300007264

Janoušek, V., Braithwaite, C. J. R., Bowes, D. R., & Gerdes, A. (2004). Magma-mixing in the genesis of Hercynian calc-alkaline granitoids: an integrated petrographic and geochemical study of the Sázava intrusion, Central Bohemian Pluton, Czech Republic. *Lithos, 78*(1-2), 67-99. doi:10.1016/j.lithos.2004.04.046

Jiang, Y., Schulmann, K., Sun, M., Štípská, P., Guy, A., Janoušek, V., et al. (2016). Anatexis of accretionary wedge, Pacific-type magmatism, and formation of vertically stratified continental crust in the Altai Orogenic Belt. *Tectonics, 35*(12), 3095-3118. doi:10.1002/2016TC004271

Karykowski, B. T., Yang, S.-H., Maier, W. D., Lahaye, Y., Lissenberg, C. J., & O'Brien, H. (2017). In situ Sr Isotope Compositions of Plagioclase from a Complete Stratigraphic Profile of the Bushveld Complex, South Africa: Evidence for Extensive Magma Mixing and Percolation. *JOURNAL OF PETROLOGY, 58*(11), 2285-2308. doi:10.1093/petrology/egy008

Kinny, P. D., & Maas, R. (2003). Lu–Hf and Sm–Nd isotope systems in zircon. *Reviews in mineralogy and geochemistry, Geophysics, Geosystems, 53*(1), 327-341. doi:https://doi.org/10.2113/0530327

Kumar, S., & Rino, V. (2006). Mineralogy and geochemistry of microgranular enclaves in Palaeoproterozoic Malanjkhand granitoids, central India: evidence of magma mixing, mingling, and chemical equilibration. *Contributions to Mineralogy and Petrology, 152*(5), 591-609. doi:10.1007/s00410-006-0122-3

Le Maitre, R., Bateman, P., Dudek, A., Keller, J., Lameyre, J., Le Bas, M., et al. (1989). A classification of igneous rocks and glossary of terms. Recommendations of the IUGS Subcommission on the Systematics of Igneous rocks. *London: Blackwell Scientific Publications*.

Leake, B. E., Woolley, A. R., Arps, C. E., Birch, W. D., Gilbert, M. C., Grice, J. D., et al. (1997). Nomenclature of amphiboles; report of the subcommittee on amphiboles of the International Mineralogical Association, Commission on New Minerals and Mineral Names. *The Canadian Mineralogist, 35*(1), 219-246.

Lesher, C. (1990). Decoupling of chemical and isotopic exchange during magma mixing. *Nature, 344*(6263), 235-237. doi:10.1038/344235a0

Li, P., Sun, M., Rosenbaum, G., Jourdan, F., Li, S., & Cai, K. (2017). Late Paleozoic closure of the Ob-Zaisan Ocean along the Irtysh shear zone (NW China): Implications for arc amalgamation and oroclinal bending in the Central Asian orogenic belt. *Geological Society of America Bulletin, 129*(5-6), 547-569. doi:10.1130/b31541.1

Long, X., Sun, M., Yuan, C., Xiao, W., & Cai, K. (2008). Early Paleozoic sedimentary record of the Chinese Altai: Implications for its tectonic evolution. *Sedimentary Geology, 208*(3-4), 88-100. doi:10.1016/j.sedgeo.2008.05.002

Miller, C. F., McDowell, S. M., & Mapes, R. W. (2003). Hot and cold granites? Implications of zircon saturation temperatures and preservation of inheritance. *Geology, 31*(6). doi:10.1130/0091-7613(2003)031<0529:Hacgio>2.0.Co;2

Müntener, O., Kelemen, P. B., & Grove, T. L. (2001). The role of H2O during crystallization of primitive arc magmas under uppermost mantle conditions and genesis of igneous pyroxenites: an experimental study. *Contributions to Mineralogy and Petrology, 141*(6), 643-658. doi:10.1007/s004100100266

Nachit, H., Ibhi, A., & Ohoud, M. B. (2005). Discrimination between primary magmatic biotites, reequilibrated biotites and neoformed biotites. *Comptes Rendus Geoscience, 337*(16), 1415-1420. doi:10.1016/j.crte.2005.09.002

Panjasawatwong, Y., Danyushevsky, L. V., Crawford, A. J., & Harris, K. L. (1995). An experimental study of the effects of melt composition on plagioclase-melt equilibria at 5 and 10 kbar: implications for the origin of magmatic high-An plagioclase. *Contributions to Mineralogy and Petrology, 118*(4), 420-432. doi:10.1007/s004100050024

Parsapoor, A., Khalili, M., Tepley, F., & Maghami, M. (2015). Mineral chemistry and isotopic composition of magmatic, re-equilibrated and hydrothermal biotites from Darreh-Zar porphyry copper deposit, Kerman (Southeast of Iran). *Ore Geology Reviews, 66*, 200-218. doi:10.1016/j.oregeorev.2014.10.015

Perugini, D., Poli, G., Christofides, G., & Eleftheriadis, G. (2003). Magma mixing in the Sithonia Plutonic Complex, Greece: evidence from mafic microgranular enclaves. *Mineralogy and Petrology, 78*(3-4), 173-200. doi:10.1007/s00710-002-0225-0

Pichavant, M., Martel, C., Bourdier, J. L., & Scaillet, B. (2002). Physical conditions, structure, and dynamics of a zoned magma chamber: Mount Pelée (Martinique, Lesser Antilles Arc). *Journal of Geophysical Research: Solid Earth, 107*(B5), ECV 1-1-ECV 1-28. doi:10.1029/2001JB000315

Poli, G., Tommasini, S., & Halliday, A. (1996). Trace element and isotopic exchange during acid-basic magma interaction processes. *Transactions of the Royal Society of Edinburgh-Earth Sciences, 87*(1), 225-232.

Putirka, K. D. (2005). Igneous thermometers and barometers based on plagioclase+ liquid equilibria: Tests of some existing models and new calibrations. *American Mineralogist, 90*(2-3), 336-346. doi:10.2138/am.2005.1449

Ratajeski, K., Glazner, A. F., & Miller, B. V. (2001). Geology and geochemistry of mafic to felsic plutonic rocks in the Cretaceous intrusive suite of Yosemite Valley, California. *Geological Society of America Bulletin, 113*(11), 1486-1502. doi:10.1130/0016-7606(2001)113<1486:GAGOMT>2.0.CO;2

Ridolfi, F., Renzulli, A., & Puerini, M. (2010). Stability and chemical equilibrium of amphibole in calc-alkaline magmas: an overview, new thermobarometric formulations and application to subduction-related volcanoes. *Contributions to Mineralogy and Petrology, 160*(1), 45-66. doi:10.1007/s00410-009-0465-7

Ruprecht, P., & Wörner, G. (2007). Variable regimes in magma systems documented in plagioclase zoning patterns: El Misti stratovolcano and Andahua monogenetic cones. *Journal of Volcanology and Geothermal Research, 165*(3-4), 142-162. doi:10.1016/j.jvolgeores.2007.06.002

Schmitt, A. K., Klitzke, M., Gerdes, A., & Schäfer, C. (2017). Zircon Hafnium–Oxygen Isotope and Trace Element Petrochronology of Intraplate Volcanic Rocks from the Eifel (Germany) and Implications for Mantle versus Crustal Origins of Zircon Megacrysts. *JOURNAL OF PETROLOGY, 58*(9), 1841-1870. doi:10.1093/petrology/egx075

Şengör, A., Natal'In, B., & Burtman, V. (1993). Evolution of the Altaid tectonic collage and Palaeozoic crustal growth in Eurasia. *Nature, 364*(6435), 299-307. doi:10.1038/364299a0

Sisson, T., & Grove, T. (1993). Experimental investigations of the role of H2O in calc-alkaline differentiation and subduction zone magmatism. *Contributions to Mineralogy and Petrology, 113*(2), 143-166. doi:10.1007/BF00283225

Sisson, T. W., Ratajeski, K., Hankins, W. B., & Glazner, A. F. (2005). Voluminous granitic magmas from common basaltic sources. *Contributions to Mineralogy and Petrology, 148*(6), 635-661. doi:10.1007/s00410-004-0632-9

Slaby, E., & Martin, H. (2008). Mafic and Felsic Magma Interaction in Granites: the Hercynian Karkonosze Pluton (Sudetes, Bohemian Massif). *JOURNAL OF PETROLOGY, 49*(2), 353-391. doi:10.1093/petrology/egm085

Snyder, D., & Tait, S. (1995). Replenishment of magma chambers: comparison of fluid-mechanic experiments with field relations. *Contributions to Mineralogy and Petrology, 122*(3), 230-240. doi:10.1007/s004100050123

Streckeisen, A., & Le Maitre, R. (1979). A chemical approximation to the modal QAPF classification of the igneous rocks. *Neues Jahrbuch Mineralogie*

Abteilung, 136, 169–206.

Sun, M., Long, X., Cai, K., Jiang, Y., Wang, B., Yuan, C., et al. (2009). Early Paleozoic ridge subduction in the Chinese Altai: insight from the abrupt change in zircon Hf isotopic compositions. *Science in China Series D: Earth Sciences, 52*(9), 1345-1358. doi:10.1007/s11430-009-0110-3

Sun, M., Yuan, C., Xiao, W., Long, X., Xia, X., Zhao, G., et al. (2008). Zircon U–Pb and Hf isotopic study of gneissic rocks from the Chinese Altai: Progressive accretionary history in the early to middle Palaeozoic. *Chemical Geology, 247*(3-4), 352-383. doi:10.1016/j.chemgeo.2007.10.026

Turnbull, R., Weaver, S., Tulloch, A., Cole, J., Handler, M., & Ireland, T. (2010). Field and Geochemical Constraints on Mafic-Felsic Interactions, and Processes in High-level Arc Magma Chambers: an Example from the Halfmoon Pluton, New Zealand. *JOURNAL OF PETROLOGY, 51*(7), 1477-1505. doi:10.1093/petrology/egq026

Ustunisik, G., Kilinc, A., & Nielsen, R. L. (2014). New insights into the processes controlling compositional zoning in plagioclase. *Lithos, 200-201*, 80-93. doi:10.1016/j.lithos.2014.03.021

Vernon, R. H. (1983). *Restite, xenoliths and microgranitoid enclaves in granites.* Paper presented at the Journal & Proceedings, Royal Society of New South Wales.

Vernon, R. H. (1984). Microgranitoid enclaves in granites—globules of hybrid magma quenched in a plutonic environment. *Nature, 309*(5967), 438-439. doi:10.1038/309438a0

Vernon, R. H. (2018). *A practical guide to rock microstructure*: Cambridge university press.

Waight, T. E., Maas, R., & Nicholls, I. A. (2000). Fingerprinting feldspar phenocrysts using crystal isotopic composition stratigraphy: implications for crystal transfer and magma mingling in S-type granites. *Contributions to Mineralogy and Petrology, 139*(2), 227-239. doi:10.1007/s004100000128

Wang, T., Hong, D.-w., Jahn, B.-m., Tong, Y., Wang, Y.-b., Han, B.-f., et al. (2006). Timing, petrogenesis, and setting of Paleozoic synorogenic intrusions from the Altai Mountains, Northwest China: implications for the tectonic evolution of an accretionary orogen. *The Journal of Geology, 114*(6), 735-751. doi:10.1086/507617

Wang, Y., Long, X., Wilde, S. A., Xu, H., Sun, M., Xiao, W., et al. (2014). Provenance of Early Paleozoic metasediments in the central Chinese Altai: Implications for tectonic affinity of the Altai-Mongolia terrane in the Central Asian Orogenic Belt. *Lithos, 210-211*, 57-68. doi:10.1016/j.lithos.2014.09.026

Wiebe, R., Blair, K., Hawkins, D., & Sabine, C. (2002). Mafic injections, in situ hybridization, and crystal accumulation in the Pyramid Peak granite, Califor-

nia. *Geological Society of America Bulletin, 114*(7), 909-920. doi:10.1130/0016-7606(2002)114<0909:MIISHA>2.0.CO;2

Wiebe, R., Smith, D., Sturm, M., King, E., & Seckler, M. (1997). Enclaves in the Cadillac mountain granite (Coastal Maine): samples of hybrid magma from the base of the chamber. *JOURNAL OF PETROLOGY, 38*(3), 393-423. doi:10.1093/petroj/38.3.393

Wiebe, R. A. (1993). The Pleasant Bay layered gabbro-diorite, coastal Maine: ponding and crystallization of basaltic injections into a silicic magma chamber. *JOURNAL OF PETROLOGY, 34*(3), 461-489.

Wilson, A. H., Zeh, A., & Gerdes, A. (2017). In Situ Sr isotopes in Plagioclase and Trace Element Systematics in the Lowest Part of the Eastern Bushveld Complex: Dynamic Processes in an Evolving Magma Chamber. *JOURNAL OF PETROLOGY, 58*(2), 327-360. doi:10.1093/petrology/egx018

Windley, B. F., Alexeiev, D., Xiao, W., Kröner, A., & Badarch, G. (2007). Tectonic models for accretion of the Central Asian Orogenic Belt. *Journal of the Geological Society, 164*(1), 31-47. doi:10.1144/0016-76492006-022

Windley, B. F., Kröner, A., Guo, J., Qu, G., Li, Y., & Zhang, C. (2002). Neoproterozoic to Paleozoic geology of the Altai orogen, NW China: new zircon age data and tectonic evolution. *The Journal of Geology, 110*(6), 719-737.

Xiao, W., Windley, B., Yuan, C., Sun, M., Han, C., Lin, S., et al. (2009). Paleozoic multiple subduction-accretion processes of the southern Altaids. *American Journal of Science, 309*(3), 221-270.

Yu, K., Liu, Y., Hu, Q., Ducea, M. N., Hu, Z., Zong, K., et al. (2018). Magma Recharge and Reactive Bulk Assimilation in Enclave-Bearing Granitoids, Tonglu, South China. *JOURNAL OF PETROLOGY, 59*(5), 795-824. doi:10.1093/petrology/egy044

Yu, Y., Sun, M., Huang, X.-L., Zhao, G., Li, P., Long, X., et al. (2017a). Sr-Nd-Hf-Pb isotopic evidence for modification of the Devonian lithospheric mantle beneath the Chinese Altai. *Lithos, 284-285*, 207-221. doi:10.1016/j.lithos.2017.04.004

Yu, Y., Sun, M., Long, X., Li, P., Zhao, G., Kröner, A., et al. (2017b). Whole-rock Nd–Hf isotopic study of I-type and peraluminous granitic rocks from the Chinese Altai: constraints on the nature of the lower crust and tectonic setting. *Gondwana Research, 47*, 131-141.

Yu, Y., Sun, M., Yuan, C., Zhao, G., Huang, X.-l., Rojas-Agramonte, Y., et al. (2018). Evolution of the middle Paleozoic magmatism in the Chinese Altai: Constraints on the crustal differentiation at shallow depth in the accretionary orogen. *Journal of Asian Earth Sciences*. doi:10.1016/j.jseaes.2018.07.026

Yuan, C., Sun, M., Xiao, W., Li, X., Chen, H., Lin, S., et al. (2007). Accretionary orogenesis of the Chinese Altai: Insights from Paleozoic granitoids.

Chemical Geology, 242(1-2), 22-39. doi:10.1016/j.chemgeo.2007.02.013

Zhang, J., Wang, T., Castro, A., Zhang, L., Shi, X., Tong, Y., et al. (2016). Multiple Mixing and Hybridization from Magma Source to Final Emplacement in the Permian Yamatu Pluton, the Northern Alxa Block, China. *JOURNAL OF PETROLOGY, 57*(5), 933-980. doi:10.1093/petrology/egw028